

OPEN ACCESS

EDITED BY
Takaaki Sokabe,
National Institute for Physiological Sciences
(NIPS), Japan

REVIEWED BY
Irfan Saadi,
University of Kansas Medical Center,
United States
Bénédicte Durand,
Université Claude Bernard Lyon 1, France

*CORRESPONDENCE
Daniel F. Eberl

☑ daniel-eberl@uiowa.edu

'PRESENT ADDRESSES
Yashoda Sharma,
Digital Medicine Society, Boston, MA,
United States
Eugene Lee,
3billion Inc., Seoul, Republic of Korea

RECEIVED 19 July 2023 ACCEPTED 07 September 2023 PUBLISHED 22 September 2023

CITATION

Sharma Y, Jacobs JS, Sivan-Loukianova E, Lee E, Kernan MJ and Eberl DF (2023) The retrograde IFT dynein is required for normal function of diverse mechanosensory cilia in *Drosophila*.

Front. Mol. Neurosci. 16:1263411. doi: 10.3389/fnmol.2023.1263411

COPYRIGHT

© 2023 Sharma, Jacobs, Sivan-Loukianova, Lee, Kernan and Eberl. This is an open-access article distributed under the terms of the Creative Commons Attribution License (CC BY).

The use, distribution or reproduction in other forums is permitted, provided the original author(s) and the copyright owner(s) are credited and that the original publication in this journal is cited, in accordance with accepted academic practice. No use, distribution or reproduction is permitted which does not comply with these terms.

The retrograde IFT dynein is required for normal function of diverse mechanosensory cilia in *Drosophila*

Yashoda Sharma^{1†}, Julie S. Jacobs¹, Elena Sivan-Loukianova¹, Eugene Lee¹, Maurice J. Kernan² and Daniel F. Eberl¹

¹Department of Biology, The University of Iowa, Iowa City, IA, United States, ²Department of Neurobiology and Behavior, State University of New York, Stony Brook, NY, United States

Introduction: Cilia biogenesis relies on intraflagellar transport (IFT), a conserved transport mechanism which functions bi-directionally to bring protein complexes to the growing ciliary tip and recycle signaling and transport proteins between the cilium and cell body. In *Drosophila*, anterograde IFT is critical for assembly of sensory cilia in the neurons of both chordotonal (ch) organs, which have relatively long ciliary axonemes, and external sensory (es) organs, which have short axonemal segments with microtubules in distal sensory segments forming non-axonemal bundles. We previously isolated the *beethoven* (*btv*) mutant in a mutagenesis screen for auditory mutants. Although many *btv* mutant flies are deaf, some retain a small residual auditory function as determined both by behavior and by auditory electrophysiology.

Results: Here we molecularly characterize the *btv* gene and demonstrate that it encodes the IFT-associated dynein-2 heavy chain Dync2h1. We also describe morphological changes in Johnston's organ as flies age to 30 days, and we find that morphological and electrophysiological phenotypes in this ch organ of *btv* mutants become more severe with age. We show that NompB protein, encoding the conserved IFT88 protein, an IFT complex B component, fails to be cleared from chordotonal cilia in *btv* mutants, instead accumulating in the distorted cilia. In macrochaete bristles, a class of es organ, *btv* mutants show a 50% reduction in mechanoreceptor potentials.

Discussion: Thus, the *btv*-encoded Dync2h1 functions as the retrograde IFT motor in the assembly of long ciliary axonemes in ch organs and is also important for normal function of the short ciliary axonemes in es organs.

KEYWORDS

cilia, intraflagellar transport, cytoplasmic dynein 1b, hearing, *Drosophila*, aging, degeneration

Introduction

The many cellular functions of cilia include motility of unicellular organisms and spermatozoa, the streaming of extracellular fluids, and signal transduction in development, homeostasis, and sensory perception. Ciliary dysfunction is associated with a correspondingly diverse set of symptoms in human disorders, such as primary ciliary dyskinesia, polycystic kidney disease, Bardet-Biedl syndrome, Joubert syndrome, and collectively termed ciliopathies (Sharma et al., 2008; Hildebrandt et al., 2011).

All cilia and membrane-enclosed flagella require intraflagellar transport (IFT) for their assembly and maintenance [reviewed by Rosenbaum and Witman (2002); Ishikawa and Marshall

(2017); Pigino (2021)]. IFT is a bidirectional mechanism that brings axoneme components to the growing tip of the cilium or flagellum and recycles signaling and transport proteins between the cilium and cell body. Movement in each direction is powered by a different processive motor protein, traveling on the polarized microtubules of the axoneme. Anterograde transport, towards the tip, is driven by plus end-directed kinesin II (Cole et al., 1998); retrograde transport is driven by a specialized cytoplasmic-type dynein complex, dynein-2 (Vuolo et al., 2020). IFT was first observed in *Chlamydomonas* as the uninterrupted movement of trains of particles along the flagellum, in the space between the axoneme and flagellar membrane (Kozminski et al., 1993). The trains include two multiprotein complexes, A and B (Cole et al., 1998), respectively composed of 6 and 16 polypeptides, most of which are conserved across all ciliated eukaryotes. The IFT-A and IFT-B complexes serve as scaffolds to organize and regulate the motors, ensuring uninterrupted movement in each direction. They are also sites of interaction with axonemal cargoes and with adaptors, such as Tulp and the BBSome complex, for ciliary membrane proteins (Jordan and Pigino, 2021; Lechtreck, 2022).

Recent studies employing cryo-electron microscopy, protein cross-linking and computational structure prediction have produced models of the A and B complexes (Hesketh et al., 2022; Meleppattu et al., 2022; Petriman et al., 2022), and of their arrangement in anterograde trains (Lacey et al., 2023). The trains have a double-decked profile, with repeated IFT-B complexes aligned next to the axoneme, overlaid by IFT-A complexes next to the ciliary membrane. Dynein-2 is carried in anterograde trains as cargo attached to the B complex, held away from the axonemal microtubules with its motor subunits in an autoinactivated configuration (Jordan et al., 2018). The retrograde train structure has not been worked out to this resolution but is clearly different in its architecture (Stepanek and Pigino, 2016), indicating that the IFT trains undergo major reconfiguration at the ciliary tip, releasing cargo, inactivating kinesin and bringing dynein-2 into play (Chien et al., 2017).

Mutations affecting motor or IFT complex proteins show ciliary phenotypes consistent with specific defects in anterograde or retrograde transport. Mutants lacking kinesin II activity or required IFT-B proteins show no anterograde transport and typically have very truncated or no cilia flagella (Cole et al., 1998; Marszalek et al., 2000; Parker and Quarmby, 2003; Sarpal et al., 2003). But in mutants with defects in dynein-2 or IFT-A proteins, anterograde transport can proceed until halted by the lack of recycled components, producing cilia that are longer but distended or distorted, in which IFT components accumulate (Criswell et al., 1996; Criswell and Asai, 1998; Pazour et al., 1999; Signor et al., 1999; Wicks et al., 2000; Mikami et al., 2002). Mutations in human *DYNC2H1*, the heavy chain subunit of dynein-2, are associated with Asphyxiating Thoracic Dystrophy (ATD) and Short-rib Polydactyly Syndrome (SRP) Type III (Dagoneau et al., 2009; Merrill et al., 2009), conditions that are consistent with ciliary dysfunction.

In *Drosophila*, ciliated cells include spermatozoa and Type I sensory neurons. Sensory neurons in chordotonal (ch) organs (also called scolopidia) exhibit long cilia with an electron-dense ciliary dilation about three fourths of the length from basal body to ciliary tip. Conversely, bristle, campaniform and olfactory organ neurons

Abbreviations: IFT, intraflagellar transport; JO, Johnston's organ; MRP, mechanoreceptor potential; SEP, sound-evoked potential; TEP, transepithelial potential.

have very short ciliary segments at the basal bodies, with loosely organized distal non-axonemal microtubule bundles. Surprisingly, although IFT is required to build sensory cilia, sperm tail assembly and maintenance in *Drosophila* appear to be independent of IFT. This conclusion is based on studies with the kinesin associated protein (DmKAP) and the motor subunit Klp64D (Sarpal et al., 2003) as well as with NompB (Han et al., 2003), the *Drosophila* homolog of IFT88/Polaris/OSM-5 (Pazour et al., 2002) and RempA, the homolog of the complex A protein IFT140 (Lee et al., 2008). In *Drosophila*, many genes required for ciliary assembly are activated by the Rfx transcription factor (Durand et al., 2000; Vandaele et al., 2001; Laurençon et al., 2007) and the forkhead-domain transcription factor Fd3F (Newton et al., 2012), but while Rfx is expressed in elongating stage spermatid nuclei (Vandaele et al., 2001) there have been no reports that either Rfx or Fd3F are required for male fertility.

Chordotonal organs participate in several sensory modalities. In Drosophila larvae, ch organs provide touch-sensitivity and proprioceptive feedback during locomotion (Kernan et al., 1994; Caldwell et al., 2003). They have also been shown to be receptive to auditory stimuli (Zhang et al., 2013; Li et al., 2021). In addition, some ch neurons are among the thermosensory neurons in the larva (Liu et al., 2003; Kwon et al., 2010). In the adult, ch organs located in the limbs and abdomen include both proprioceptive and vibrosensory neurons (Fabre et al., 2012; Mamiya et al., 2018). Wing ch organs provide feedback not only during flight, but also during courtship song production (Tauber and Eberl, 2001). Johnston's organ (JO), the antennal ch organ, functions as the auditory organ (Eberl et al., 2000). It is also responsible for gravity and wind sensing (Armstrong et al., 2006; Kamikouchi et al., 2009; Sun et al., 2009; Yorozu et al., 2009). Chordotonal organs in the adult also contribute to temperature entrainment of adult circadian rhythms, though JO is not required for this function (Sehadova et al., 2009).

The phenotypes we previously described for the beethoven (btv) mutation (Eberl et al., 1997, 2000; Tauber and Eberl, 2001; Caldwell et al., 2003), together with mapping data, suggested that Dync2h1, the retrograde motor for *Drosophila* IFT, was a good candidate gene. Here we demonstrate that btv is the predicted gene CG15148, which encodes the Dync2h1 homolog. We show that btv is required for ciliary assembly in ch organs, and that morphological and electrophysiological phenotypes of btv mutants become more severe with age. To support the notion that the Dync2h1 encoded by btv actually participates in retrograde IFT, we show that NompB, an IFT complex B protein, fails to be cleared from the chordotonal cilium in btv mutants. Finally, we show that the btv mutation also reduces mechanoreceptor potentials (MRPs) of bristle organs by about 50% without affecting trans-epithelial potentials (TEPs), suggesting that retrograde IFT plays a role in external sensory (es) organs despite the shortness of these axonemal segments (Table 1).

Materials and methods

Fly strains and crosses

Drosophila melanogaster mutants of *btv* used in this study are listed in Table 1. For P-induced male recombination, the transposase source was supplied by w^+ ; *Sp btv¹ pr rl cn/CyO*; *Dr P {\Delta 2-3}/TM6*, *Ubx*. The *Sternopleural (Sp)* and *purple (pr)* genes are used as flanking

TABLE 1 Genetic variants used in this study.

<i>btv</i> genotype	Synonyms	Molecular defect	DZA score	Hearing	Remarks	References
btv ⁺	40AG13	None		Normal	Control for btv ¹	Eberl et al. (1997, 2000)
btv ¹	btv ^{5P1}	401 bp deletion/6 bp insertion, intron 12–13 into exon 13	4.79	Severe	EMS-induced	Eberl et al. (1997, 2000); this work
btv ²	btv ^{k07109b}	Frameshift caused by single nucleotide deletion of A in exon 22, coordinate 17,966,613		Severe	P-induced; not associated with P-inserts	Spradling et al. (1999), Mancebo et al. (2001), Bellen et al. (2004) and Comeron et al. (2016); this work
Df(2 L)TW119/ Df(2 L)TW201		Homozygous deficient from CadN2 to rdo	5.0; 5.4	Severe	Viable, and show rdo phenotype; male sterile due to other loci	Eberl et al. (2000)
btv ³	BG01771	P-insert, intron 13–14	1.5; 1.0; 1.89	Normal	P{GT1} insertion (dual-tag)	Bellen et al. (2004); this work
btv ⁴	btv ^{I.f234}	3,196 bp deletion of exons 12–13; 1 bp insertion (G)	5.0	Severe	P-induced; 2nd-site lethal; tested over btv ¹	This work
btv ⁵	f06884	PBac insert, exon 23		Severe	PBac{WH} insertion	Thibault et al. (2004)
btv ⁶	f06878	PBac insert, intron 13–14		Normal	PBac{WH} insertion, 6 bp left of the BG01771 insertion site	Thibault et al. (2004)
del#1		Deletion of DNA between f06884 and f06319 insertion sites		Severe	deletes 3' end of Dync2h1 leftward	This work
del#2		Deletion of DNA between f06878 and f06603 insertion sites		Severe	deletes 5' end of Dync2h1 rightward	This work

markers to map btv. These flies were crossed to w/Y; P {GT1}BG01771 males. Dysgenic male offspring were crossed to w^+ ; Df(2L)TW12 Tftpr/CyO, pr females to recover Sp pr or Sp pr recombinants. Recombinants were subsequently tested for btv genotype by crossing to w; btv1 40AG13/CyO. Df (2L)TW12 is unrelated to the btv region, while *Tufted* (*Tft*) is a dominant bristle marker. A total of 5,966 flies (250 pair matings) were screened and 9 male recombinants recovered (Supplementary Table S1), giving a recombination rate of 0.15%. To recover putative deletions between the BG01771 insertion and the insertion sites of nearby P-element insertions KG02815 or KG08320, the BG01771 insertion was first crossed to flies containing the transposase source, w^+ ; Sp/CyO; P { $\Delta 2$ -3} Sb/TM6, Ubx. Resulting w^+/w ; BG01771/Sp; +/P { $\Delta 2$ -3} Sb females were crossed to either w^+/Y ; KG02815 or w^+/Y ; KG08320 males. Dysgenic w/Y; BG01771/KG; +/P $\{\Delta 2-3\}$ males were crossed to w; Sco/CyO females and the offspring screened for white eyes. About 330 putative deletions were crossed to w; btv1 40AG13/CyO to test for btv phenotype.

Behavioral assay: drop zone assay

To measure sedentary behavior and associated loss of flight ability, we developed the drop zone assay (DZA; Supplementary Figure S2). A square plexiglass cover, with a hole in its center, was placed on top of a 4liter glass beaker. Flies were introduced in groups of 10 through the hole into the beaker, observed for 1 min and assigned a score from 1 to 6 as follows. Score 1: the fly did not touch the beaker bottom but flew directly upwards and landed on the plexiglass ceiling. Score 2: the fly landed on the beaker wall and climbed to the top. Scores of 3, 4, 5, or 6: the fly fell to the beaker floor, and either climbed immediately

more than halfway to the top (3), climbed less than mid-way to the top (4), did not climb, but wandering around the beaker floor (5), or remained at the landing position (6).

Electrophysiology

Extracellular recordings used to assay the sound-evoked potentials (SEPs) in the antennal nerve were performed as previously described (Eberl et al., 2000; Eberl and Kernan, 2011). Transepithelial potentials (TEP) and mechanoreceptor potentials (MRP) were recorded from adult anterior notopleural bristle organs essentially as previously described (Kernan et al., 1994), except that decapitated flies were mounted on a chlorided silver pin, which served as the basal electrode; transepithelial potentials were recorded with an EPC7 amplifier (List Medical) in current-clamp mode, and data was acquired and analysed with Powerlab/LabChart (AD Instruments). TEP values are relative to a zero obtained by inserting the bristle electrode into the body cavity, in cisepithelial configuration. The MRP was calculated as the maximal absolute change in TEP within 100 ms of the stimulus onset. Adaptation was calculated as the difference between the minimum TEP reached and the TEP averaged over the last 200 ms of a 1s stimulus, as a percent of the MRP.

Electron microscopy

Drosophila heads, with proboscii removed to facilitate infiltration, were fixed by immersion overnight at 4° C in a fixative containing 2.5% glutaraldehyde, 2.0% paraformaldehyde and 0.04% CaCl₂ in

 $0.1\,\mathrm{M}$ phosphate buffer, pH 7.4 (PB). CaCl₂ provides increased membrane stabilization. Heads were washed in PB, post-fixed with OsO₄, dehydrated in an ethanol series and embedded in Polybed 812. Ultrathin sections (75 nm) were stained with aqueous uranyl acetate and lead citrate and examined with a Hitachi 7000 electron microscope.

Fluorescent staining and imaging

The fluorescently-tagged IFT proteins IFT88 [GFP-NompB (Han et al., 2003)] and IFT140 [RempA-VenusYFP (Lee et al., 2008)], expressed from transgenes, were imaged in situ by their native fluorescence, in combination with immunolabelling of the proteins Futsch or NompA. Pupal antennae or pupal or pharate adult abdomen and halteres were dissected in PBT (0.2% Triton-X in PBS) and fixed in 4% formaldehyde in PBT. After three 10 min washes in PBT, specimens were incubated in blocking solution (PBT with 5% normal goat serum) for 1 h at room temperature. Futsch was labelled by incubating with mAb 22C10 (Developmental Studies Hybridoma Bank, Iowa City, IA) at a 1:100 dilution for 2.5 h at room temperature, followed by incubation with Alexa Fluor 546-conjugated goat antimouse antibody (Invitrogen) at 1:500 dilution, for 2 h, also at room temperature. NompA was labelled with rabbit anti-NompA (Chung et al., 2001) at a 1:500 dilution, followed by incubation with Alexa Fluor 647-conjugated goat anti-rabbit (Invitrogen) at 1:500 dilution. Specimens were mounted with Vectashield mounting media (Vectorlabs, CA) on a microscope slide and examined with a confocal microscope (Leica SP5).

Southern analysis, PCR, and sequencing

Genomic DNA was isolated from adults and digested with EcoRI, HindIII or XhoI, run on agarose gel, and transferred to Hybond membrane according to instructions provided with the membrane. Southern blot analysis was performed using DIG High Prime DNA Labeling and Detection Starter Kit I (Roche) according to manufacturer's instructions. A dot blot was conducted to confirm labeling and determine the concentration of labeled probe.

Primers presented in figures and used in PCR reactions include:

Se13F: 5'-ACTTGTTATCGTCCAACACC-3'. Dhc9R: 5'-GTGCCAGCAGAACTTGATGA-3'.

PS5F: 5'-CAGCAACATCATCTGCAGCA-3'.

PS7R: 5'-ATAAGAATGCGGCCGCAATCTACAGGCGAC-3'.

Results

The btv1 mutation strongly reduces hearing and affects chordotonal ciliary structure

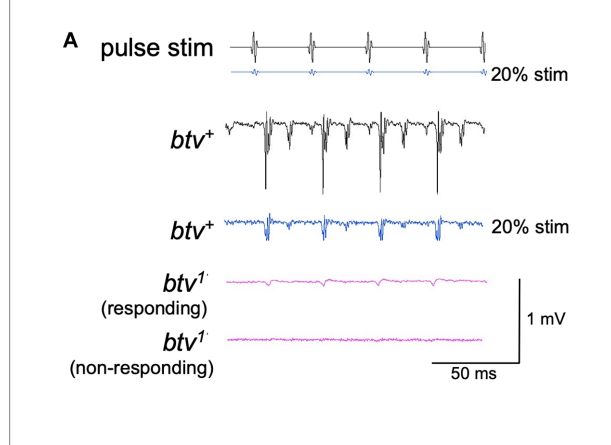
In a behavioral mutagenesis screen (Eberl et al., 1997), we isolated a mutant, 5P1, with reduced courtship song response. This mutant showed severely disrupted sound-evoked potentials (SEPs) in the antennal nerve (Eberl et al., 2000) and the corresponding gene was named beethoven (btv), with the btv^{5P1} allele also referred to as btv^1

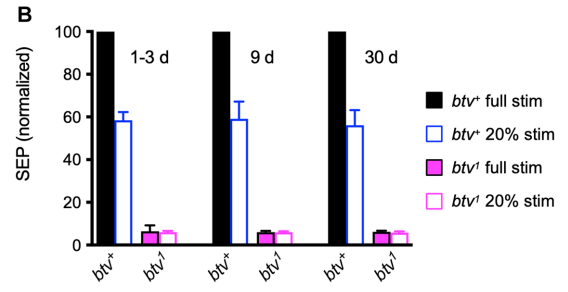
(Caldwell et al., 2003). Most btv^I mutant flies retained a small SEP, especially if subjected to loud sound (Eberl et al., 2000), consistent with retention of a residual behavioral response to courtship song presentation (Eberl et al., 1997). This appears to be the null phenotype because overlapping deletions that remove the btv locus (such as Df(2L)TW119/Df(2L)TW201) also retain this residual SEP. To better understand the mutant phenotype, we examined the ciliary structure in more detail, and tested whether the residual response represented degeneration in progress. Thus, we compared electrophysiological phenotypes of btv mutants to controls 1–3 days after eclosion, after 9 days, and after 30 days. As btv^+ control flies, we used the genetic background on which the btv^I mutation was induced (Table 2; Eberl et al., 1997). This strain, like the Canton-S wild-type strain, shows a general age-dependent decline in SEPs (Supplementary Figure S1) though little change before 30 days of age.

Consistent with our previous results, we found that many, but not all, btv^l flies showed small SEPs in response to a standard pulse song stimulus (Figure 1A). At a lower (20%) stimulus intensity, control flies showed SEPs of about 55% of their response to the standard amplitude regardless of age up to 30 days (Figures 1A,B). In contrast, average SEPs of btv^l mutants were the same at loud and soft stimuli (Figure 1B). Therefore, we scored the percent of antennae that showed any detectable response. Compared to control flies, in which all antennae showed evoked responses, less than 40% of btv^l antennae showed a response at 1–3 days, declining to less than 10% by 30 days (Figure 1C). Thus, the residual auditory function seen in btv^l flies undergoes an early age-dependent decline.

To investigate in more detail the morphological effects on JO scolopidia resulting from loss of btv function, and to examine the degenerative effects at the morphological level, we used TEM to characterize JO scolopidia from control and mutant flies at 1-3 days, 9 days and 30 days old (Figures 2-4). The normal structure of an individual JO scolopidium is diagrammed in Figure 2, with TEM sections showing the inner and outer dendritic segments of the neuron, including the ciliary rootlet, the basal bodies, the proximal ciliary segment (bearing dynein arms), the ciliary dilation and the distal ciliary segment (lacking dynein arms). The scolopale cell, supported by actin-rich scolopale rods with embedded microtubules, encloses the sensory cilia within an extracellular cavity called the scolopale space, which likely contains a specialized receptor lymph to drive receptor potentials during mechanotransduction. The scolopale cell secretes NompA protein (Chung et al., 2001) into the extracellular matrix to form the dendritic cap, which connects the neuronal ciliary tips to the a2/a3 joint cuticle. A cap cell surrounds the distal end of the scolopale cell and enwraps the dendritic cap, but it is unclear whether it contributes proteins to the dendritic cap structure.

In the btv^I mutant, we saw no significant changes to the inner dendritic segment at any of the ages tested, compared to control. The inner dendritic segments are tightly associated by desmosomes, both with each other and with scolopale rods in the apposed scolopale cell, and the base of the cilium always contains proximal and distal basal bodies and a ciliary root (Figure 3B). Near the basal bodies, the axoneme is usually complete with the expected nine microtubule doublets (Figure 3B). Beyond the ciliary base, the sensory cilia of btv^I mutants show some segments constructed reasonably well, while other segments are fragmented and disorganized (Figure 3D) compared to btv^I controls (Figures 3A,C). At the mid-scolopale level of btv JO at all ages examined, we found frequent loss of microtubule





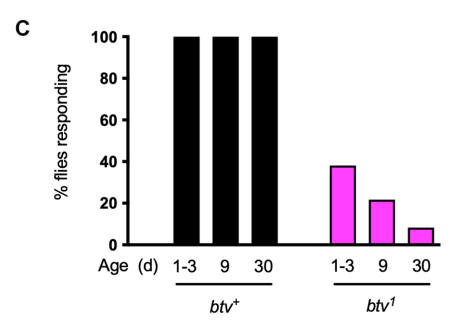


FIGURE 1

Electrophysiological phenotypes of btv mutant. (A) Sound-evoked potentials (SEPs) recorded from the antennal nerve, in response to near-field presentation of computer-generated sound stimulus (pulse stim) with 35 ms inter-pulse interval. The 40AG13 control strain (btv+) shows robust SEP (~1 mV) responses to the stimulus pulses at standard intensity. With the electrode position unchanged presenting the same stimulus at lower intensity (20%, blue stimulus) still evokes a recognizable response with lower amplitude (blue response trace). Responses of btv1 flies are somewhat variable, with some antennae showing a detectable, though low amplitude response (responding), and some antennae, particularly in older flies, showing no response (non-responding). (B) Quantitative SEP analysis with age. Filled bars represent responses to the standard sound intensity stimulus; open bars represent responses to the 5-fold lower stimulus amplitude. For normalization, the mean for btv+ at normal intensity was set at 100% for each age group. The number of antennae recorded at 1-3, 9, and 30 days were 42, 16, and 21, respectively, for btv+, and 27, 25, and 36 for btv1. (C) Refer to key in panel (B). While the mean SEPs appear very similar between the normal and 5-fold reduced stimulus in btv1 flies and over the three age groups (B), the percent of btv1 flies with a recognizable response (see A) decreases with age

doublets and loss of ciliary membrane (Figures 3E–J), often resulting in very deformed ciliary profiles (Figures 3G,J). Despite these defects, we often see clear dynein arms present on the axonemes (Figure 3G). At the expected location of the ciliary dilation, about three fourths of

the distance from the basal bodies to ciliary tip (Figure 4A), we never see the organized grid-shaped matrix of the ciliary dilation in btv flies. Instead, we sometimes observe a complex of additional membranes, vacuoles and microtubules embedded in electron dense material (Figure 4B).

We were surprised to find, in control animals, excess membranes accumulating in the scolopale space with age. The appearance of these membranes varies from scolopidium to scolopidium, from loosely organized membranous material floating in the scolopale space (Figure 4A) to robust vacuoles whose expansion occludes the cilia to the edge of the space, as in btv (Figure 3E). To ensure that this is not specific to our control strain, 40AG13, we checked the Canton S wild-type strain and found similar levels of membrane accumulation in the scolopale space with age (not shown). These membranes are similar in btv mutants and control flies; however, in btv flies 9 days and older, the ciliary occlusions are sometimes accompanied by deformation of the ring of scolopale rods, and even invagination of membranes between scolopale rods, resulting in crescent-shaped scolopidial profiles (Figure 3H). In addition, only in the btv mutants, starting at the 9 day time-point, we begin to see additional elongated tubular structures (Figures 3D,I,J) that resemble strings of sausages. These accumulations may correlate with fewer ciliary profiles at 30 days (Figure 4B), and therefore may represent degenerating ciliary material. Alternatively, the appearance of membranous vesicles in the scolopale space may be caused by ciliary vesicle shedding (Ojeda Naharros and Nachury, 2022), which could be enhanced upon loss of retrograde IFT. The effects of age on control and mutant scolopidia are summarized in Table 2. To test whether the degenerative effects could result from activation of apoptosis, we stained sections of 14 day old btv mutant and control antennae with the TUNEL technique, and found no difference in labeling (not shown), suggesting that the consequences of age on btv mutants are not apoptotic in origin.

Isolation and mapping of beethoven mutations

To understand the molecular basis of the btv phenotype, we pursued identification of the *btv* gene. Therefore, we carried out a series of genetic mapping studies and isolated several new alleles. As we shall describe, *btv* is identical with *Dhc36D* (also called *DHC1b* and *CG15148*), and encodes the retrograde IFT dynein motor, Dync2h1. Henceforth, we will use *Dync2h1*, according to the nomenclature proposed by Braschi et al. (2022). Because the *Dync2h1* gene is strongly mutually nested with the *CG5674* gene, it was critical that we used multiple approaches to conclusively determine whether *btv* corresponds to *Dync2h1*. This analysis is summarized below and in Figure 5 and described in additional detail in the Supplementary Material.

First, we mapped the *btv*¹ allele isolated in an ethyl methanesulfonate (EMS) mutagenesis screen (Eberl et al., 1997) to the 36E1-3 polytene chromosome region to the left of the *rdo* locus by deficiency mapping (Eberl et al., 2000; Caldwell et al., 2007) (Figure 5). Using *P*-induced male recombination (PIMR) (Chen et al., 1998), we refined the *btv* map position to the right of the *KG08320 P*-element (Figure 5 and Supplementary Table S1). Next, while the *P* {*GT1*} *BG01771 and PBac* {*WH*} *f06878* insertions (Figure 5C) do not show

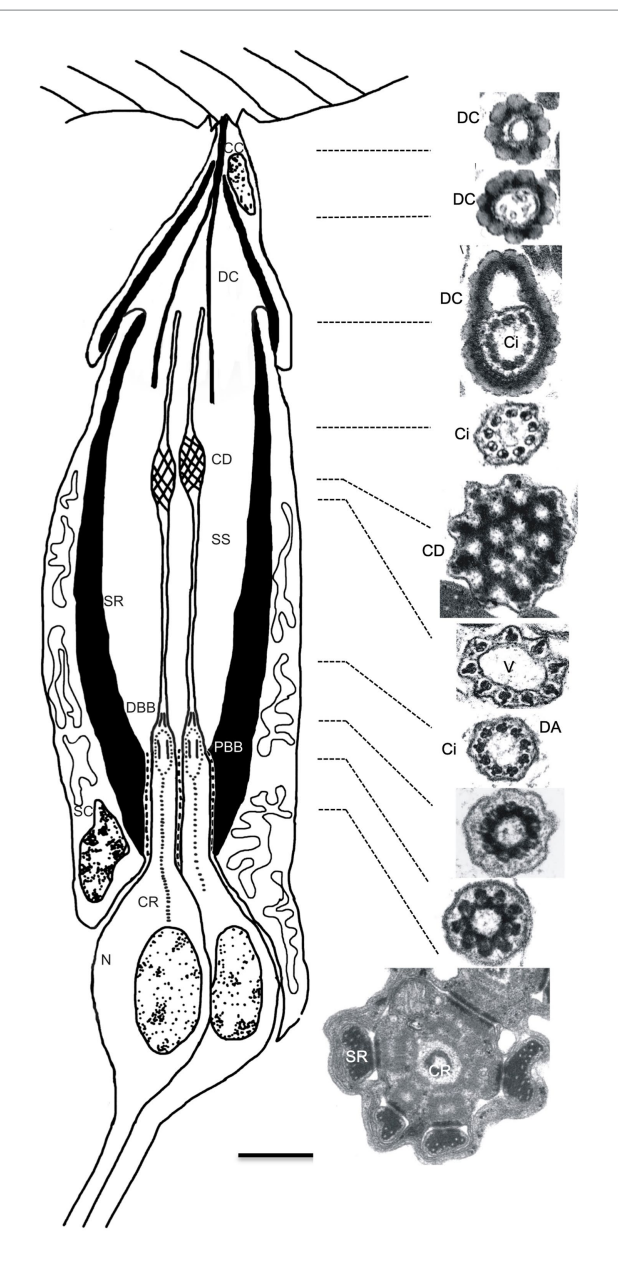


FIGURE 2

Structure of Johnston's organ scolopidium in the wild type. Diagram (left) shows the cellular composition of a JO scolopidium, with apical attachment to the a2/a3 joint cuticle (top). The scolopale cell (SC) tightly envelops dendritic ends of neuronal cells (N), forming a scolopale space (SS) thought to contain a specialized receptor lymph. Apically, the cap cell (CC) surrounds the dendritic cap (DC) and seals the distal end of the scolopale space. Both the scolopale cell and the cap cell contain thick bundles of actin, called scolopale rods (SR), which form around a microtubule core. The neuronal dendrites are sensory cilia that grow out from the centriole-derived basal bodies [proximal and distal basal bodies (PBB and DBB)] and show long prominent ciliary roots (CR) that usually reach to the soma, and sometimes beyond into the axon. The sensory cilium (Ci) is subdivided into proximal and distal segments by the ciliary dilation (CD). Electron micrographs show cross-sections of the dendritic cap and a single sensory dendrite at the approximate levels indicated by the dotted lines. In sequence from the top, the electron micrographs on the right side show the beaded appearance of the dendritic cap (top 3 images) and variations in appearance of the dendrite. Within the dendritic cap, the distal cilium is closely associated with the cap material. The ciliary dilation (5th image from top) shows the expanded ciliary diameter, inclusion of an electron-dense matrix, and 9 peripheral microtubule doublets, which spread to continue around the dilation. Immediately below the dilation, and sometimes above as well, a vacuole space (V) appears as the microtubule doublets taper down to the normal ciliary diameter (6th image). Axonemal dynein arms (DA) are present in the ciliary segment below the ciliary dilation, especially visible in the 7th image, but not in the segment above the dilation (4th image). The bottom 3 images show the cross-sectional appearance proximal to the ciliary axoneme. The upper of these 3 images is at the transition from the distal basal body to the cilium, while the middle image depicts the proximal ciliary transition zone. The lowest image shows the inner dendritic segment with the central ciliary root. Scale bar (0.5 µm) applies to all electron micrographs. Diagram is not drawn to scale; the dendritic cap and cap cell are several times the length of the sensory cilia, but are shortened here for clarity.

a btv phenotype, btv⁵, the PBac {WH}f06884 insertion in exon 23 of Dync2h1 (Figure 5C and Table 1), fails to complement other btv alleles. Using a variety of strategies (see details in

Supplementary Material), we generated several additional mutations, including btv^4 , del#1, and del#2, which likely affected both Dync2h1 and CG5674.

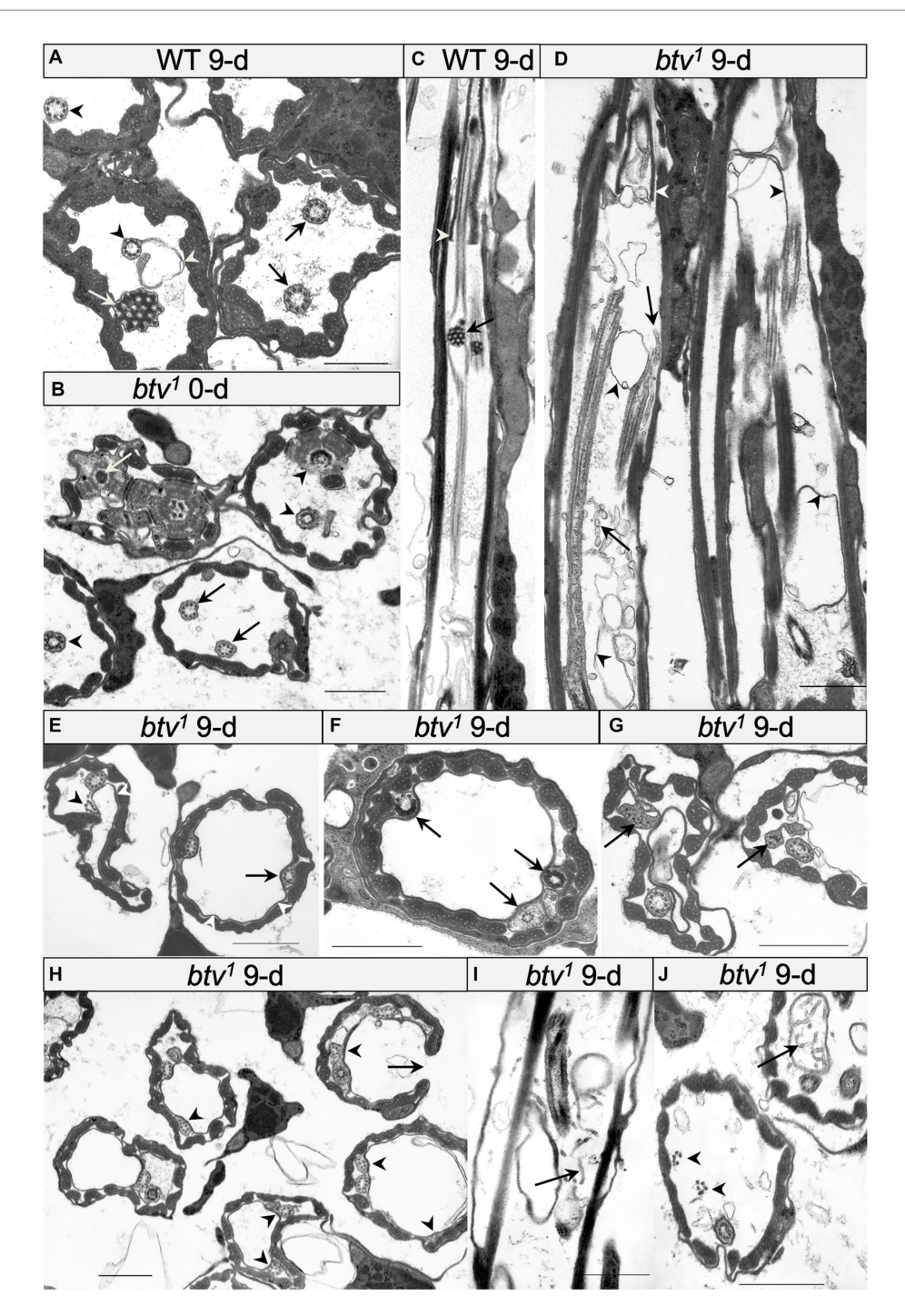


FIGURE 3

Morphological defects in btv and control JO scolopidia. (A) Cross-section through JO scolopidia of 9 days-old wild-type fly shows typical electrondense ciliary dilation (white arrow), cilia bearing dynein arms (black arrows) proximal to the ciliary dilation, and cilia lacking dynein arms (black arrowheads) distal to the ciliary dilation. A small amount of excess membrane (white arrowhead) can sometimes be seen in the wild type. (B) Crosssection through proximal JO scolopidia of newly eclosed btv1 fly shows many normal inner dendritic structures including ciliary rootlet (white arrow), and basal bodies (black arrowheads) but the proximal axonemal segments (black arrows) sometimes show fewer than 9 microtubule doublets. dilation with electron-dense matrix (black arrow) is visible, along with a grazing section nearby through the ciliary dilation of the second neuron. Beyond the ciliary dilation, the cilium is enclosed by the dendritic cap (white arrowhead). (D) Longitudinal section through two 9-day-old btv mutant scolopidia. Variable ciliary assembly is revealed by segments of these cilia. Some ciliary material is associated with the dendritic cap (white arrowhead). Extra membranous material (black arrowheads) appears in the scolopale space, and some fragmented material (black arrow) that may be degenerating $axonemes, appears \ as \ "sausage-like" \ structure. \ (\textbf{E}-\textbf{G}) \ Cross-sections \ at \ mid-scolopale \ level \ of 9 \ days-old \ \textit{btv}^{L} \ JO. \ Excess \ membranes \ fill \ the \ scolopale \ level \ of 9 \ days-old \ \textit{btv}^{L} \ JO. \ Excess \ membranes \ fill \ the \ scolopale \ level \ of 9 \ days-old \ \textit{btv}^{L} \ JO. \ Excess \ membranes \ fill \ the \ scolopale \ level \ of 9 \ days-old \ \textit{btv}^{L} \ JO. \ Excess \ membranes \ fill \ the \ scolopale \ level \ of 9 \ days-old \ \textit{btv}^{L} \ JO. \ Excess \ membranes \ fill \ the \ scolopale \ level \ of 9 \ days-old \ \textit{btv}^{L} \ JO. \ excess \ membranes \ fill \ the \ scolopale \ level \ of 9 \ days-old \ \textit{btv}^{L} \ JO. \ excess \ membranes \ fill \ the \ scolopale \ of 9 \ days-old \ days-o$ space (white arrowheads), often pushing the cilia to the edge. Axonemes show a variety of disruptions (black arrowheads) such as lack of enclosing ciliary membrane, fewer than 9 microtubule doublets, unusual electron-dense inclusions or more severe ciliary disruptions. (H) Cross-sections through a 9 days-old btv¹ JO at mid-scolopale level, showing scolopale disruptions that include occasional crescent-shaped scolopale profiles (arrows). Many axonemes are missing microtubule doublets (arrowheads). (I, J) Longitudinal (I) and cross-sections (J) of 9 days-old btv¹ JOs show abnormal accumulations of tubular material (arrows). The origin of this "sausage-like" material is unknown, but may represent degenerating axonemal derivatives. A fragmented axoneme (arrowheads) is seen lacking a ciliary membrane. All scale bars are 1 µm.

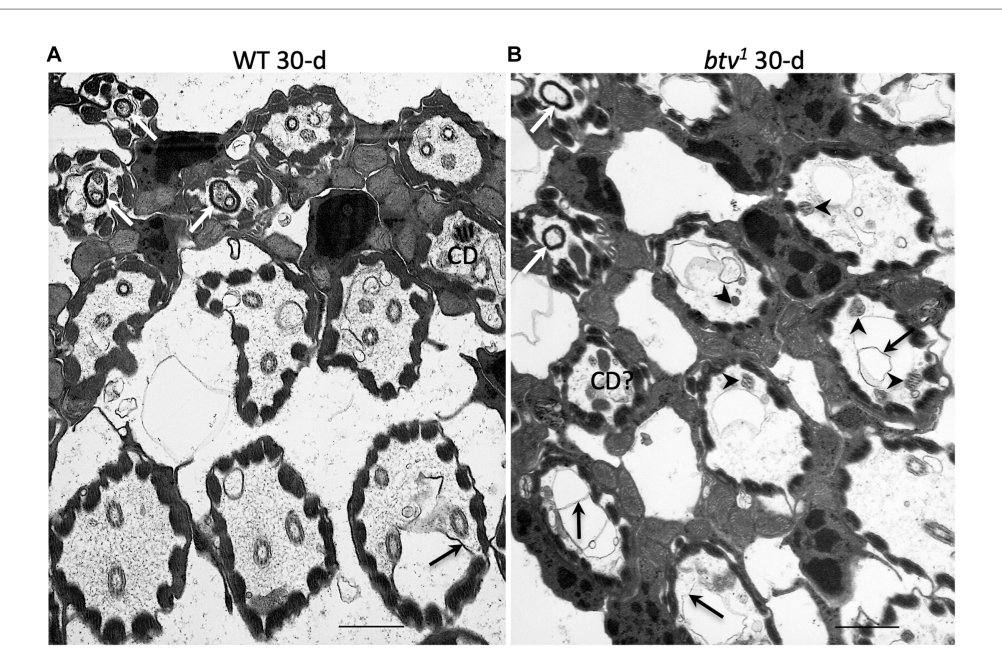


FIGURE 4

JO scolopidial structure in 30 days-old control and *btv* mutants. Slightly oblique sections through fields of JO scolopidia reveal structure at several levels from mid-scolopale (bottom right) to dendritic cap level (top left) in a control fly (**A**) and a *btv*¹ mutant (**B**), both 30 days old. (**A**) The control scolopidia each show two or three sensory cilia within the scolopale space. One ciliary dilation (CD) is sectioned through its electron dense core, and three dendritic caps (white arrows) are seen in the upper left, enclosing ciliary tips. While some excess membrane (black arrow) is seen occasionally, ciliary integrity is maintained. (**B**) The *btv*¹ mutant at 30 days shows strong ciliary defects above the basal body level. Most scolopidia have only fragmented axonemes (arrowheads), if any. Some electron dense material that may represent degenerate ciliary dilations can be seen in some distal scolopale spaces (CD?), and beyond that, the dendritic caps (white arrows) appear mostly empty or enclosing only amorphous material. Scale bars: 1 µm.

TABLE 2 Summary of age effects on control and $\it btv$ mutant JO scolopidial structure.

Feature	Contro	ol	btv¹	
	Young	Old	Young	Old
1. Ciliary dilation	+	+	_	_
2. 9×2 arrangement of microtubule doublets	+	+	_	_
3. Cap structure	+	+	_	_
4. Additional membranes	+	+/-	_	_
5. Membrane loops at ciliary dilation	+	+	_	_
6. Scolopale invaginations	+	+/-	_	_
7. "Sausage-like" structure	+	+	+	_

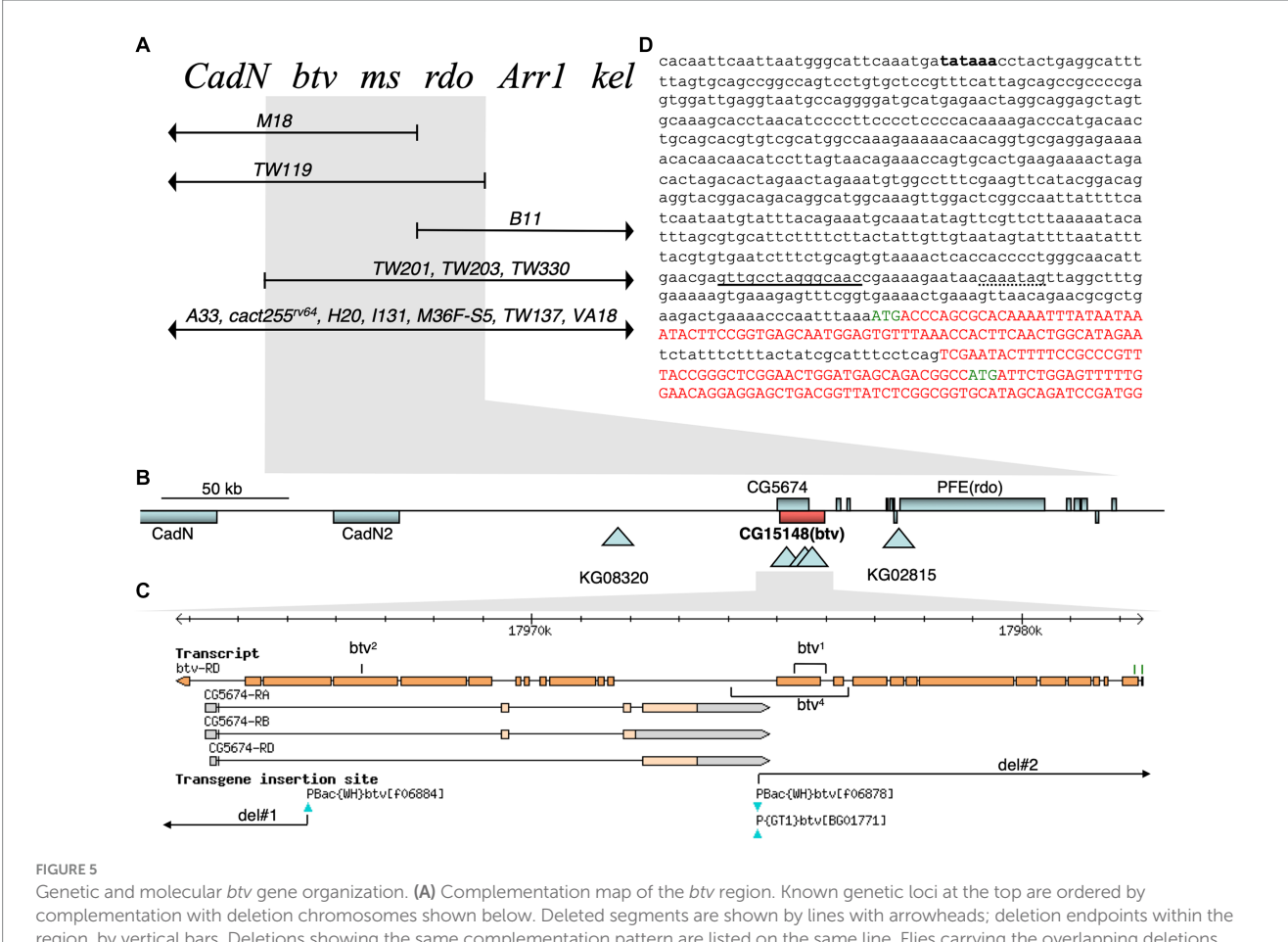
For each phenotype, "+" indicates normal; "-" indicates defective; "+/-" indicates a mix of normal and defective scolopidia; "--" indicates strongly defective. "Young" refers to the phenotype of 1-3 day old flies, while "old" refers to 30 days old flies.

Because the btv^{l} mutation was generated by EMS, we expected to find a point mutation. Further characterization, however, revealed a 401 bp deletion along with a 6 bp insertion (Figure 6C). The deletion removes 125 bp of Dync2h1 exon 13 and part of the intron between exons 12 and 13. Because this deleted region excludes any CG5674 sequences, the btv^{l} lesion firmly establishes Dync2h1 as btv. This is supported by our discovery in btv^{2} , using Mismatch Endonuclease Arrays (MENA) (Comeron et al., 2016), of a single nucleotide deletion in Dync2h1 exon 22 resulting in a frameshift that introduces an early stop codon (Comeron et al., 2016). This position is in the middle of a large intron in the overlapping gene CG5674 on the opposite strand, and therefore

unlikely to affect its function (Figure 5C). Finally, we found numerous sequence polymorphisms in different lab strains compared to the sequence used for the genome annotation (Supplementary Table S1), emphasizing the need to compare sequence deviations relative to the background strain on which the mutation was induced.

We find no differences in the electrophysiological phenotypes between btv alleles that also disrupt CG5674 and those that do not. Thus there is no evidence that CG5674 contributes to the btv phenotype.

Taken together, all these observations demonstrate that the *btv* gene corresponds to *Dync2h1*.



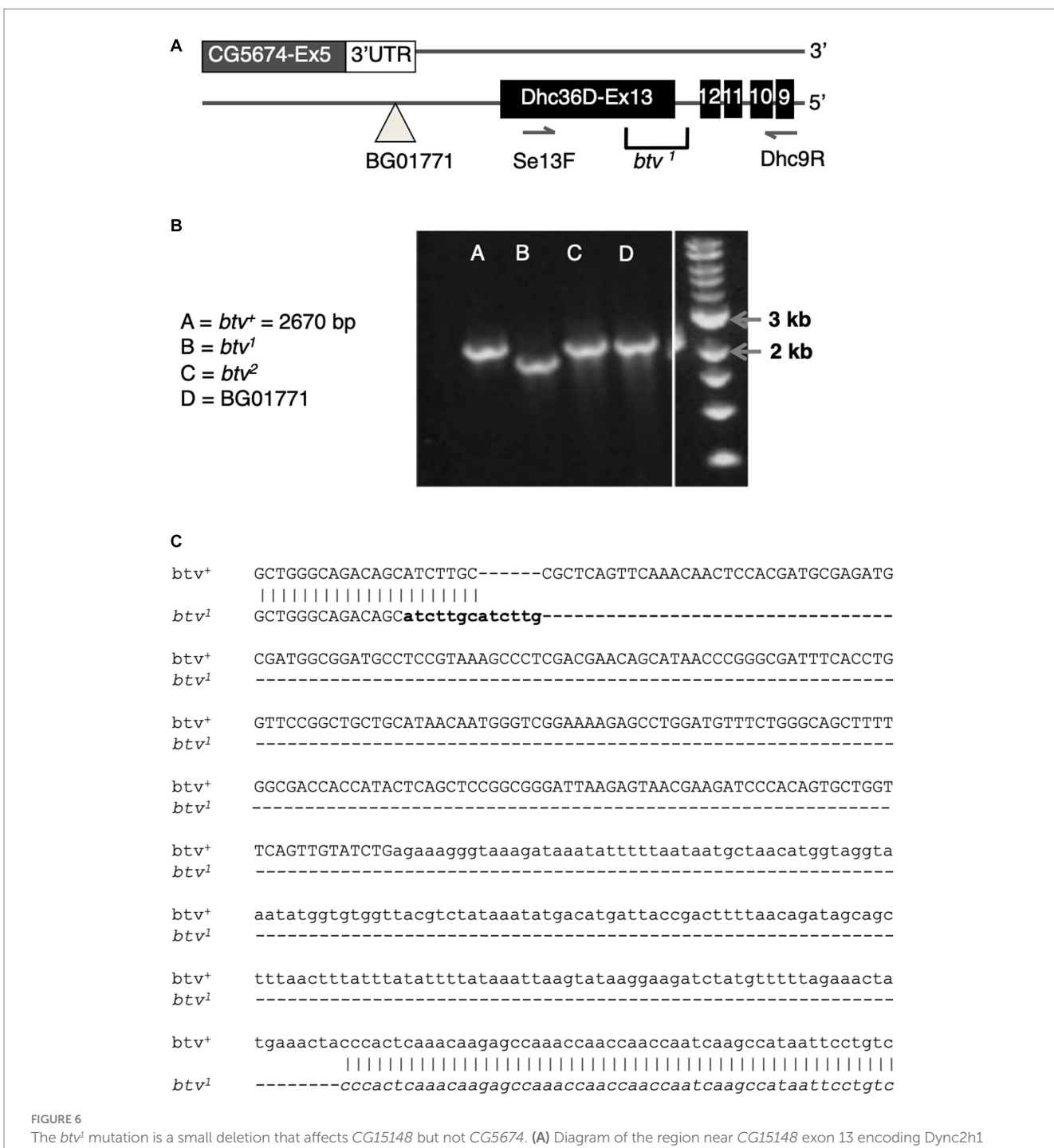
Genetic and molecular *btv* gene organization. (A) Complementation map of the *btv* region. Known genetic loci at the top are ordered by complementation with deletion chromosomes shown below. Deleted segments are shown by lines with arrowheads; deletion endpoints within the region, by vertical bars. Deletions showing the same complementation pattern are listed on the same line. Flies carrying the overlapping deletions *TW119* and *TW201* are viable, show the btv and rdo phenotypes, and are male sterile. The *btv* mutation is rescued by *Dp (2; Y)H3* (not shown).

(B) Physical map of *btv* genomic region. Gene spans are shown as rectangles: genes above the line are transcribed to the right; those below, to the left. Triangles indicate transposon insertion sites. (C) JBrowse view of the *btv* gene, with exons represented by orange rectangles. Two putative *btv* translation start sites are indicated as green tick marks. All exons of the oppositely transcribed gene *CG5674* are fully nested within the *btv* introns. Transposon insertions are indicated below. Positions of the small deletions in *btv*¹ and *btv*⁴ are indicated, as are the FRT-mediated deletions (*del#1* and *del#2*). (D) Genomic sequence at 5' end of *btv* gene. Putative coding sequences are shown in upper case red or green letters, with green letters indicating the two putative translation starts. The 29 base pair intron between exons 1 and 2 has not been experimentally confirmed. A perfect consensus X-box sequence for Rfx transcription factor binding is shown with dotted underline (Newton et al., 2012). A putative upstream TATA box sequence is in bold font but has not been functionally confirmed.

Beethoven encodes the retrograde IFT dynein motor

All our evidence indicates that *btv* corresponds to *CG15148*, which encodes a dynein heavy chain most similar to members of the Dync2h1 isoform. The annotated intron-exon structure and protein sequence evolved significantly over the course of this project. We sequenced PCR amplicons from cDNA of adult heads from 40AG13 and *w*¹¹¹⁸ control strains to define the intron-exon structure. Each amplicon was generated at least two independent times to distinguish sequence changes from PCR-induced changes. The current annotation (*D. melanogaster* r6.50; Gramates et al., 2022) resembles our empirical data most closely. Exons 2–24 (Figure 5C) match our cDNA sequencing results. We did not confirm exons 1 and 25, reported in the annotation. However, protein sequences predicted in exon 1 retain considerable conservation with Dync2h1 isoforms from other insects, and some modest conservation with vertebrate homologs. Upstream of the putative starting methionine in exon 1 (Figure 5D), we found a putative TATA box at about 635 bp

upstream, and a perfect match to a Rfx transcription factor binding site consensus at about 100 bp upstream and to a Fd3F consensus site about 90 bp upstream (Laurençon et al., 2007; Cachero et al., 2011; Newton et al., 2012). This is consistent with Rfx-dependent (Laurençon et al., 2007) and Fd3F-dependent (Newton et al., 2012) regulation of btv. While the starting methionine in exon 1 is more likely correct, a second possible starting methionine is present in exon 2 (Figure 5D; Supplementary Figure S4). Protein sequences predicted from exon 25 share similarity with closely related insect homologs but not with vertebrate homologs. However, until the splicing structure is confirmed experimentally, we cannot be certain of the structure at the C-terminus. Assuming the longest prediction, the protein would consist of 4,237 amino acids, for a predicted molecular weight of 481.45 kDa, barring posttranslational modifications (Supplementary Figure S4). Consistent with the structure of other dynein heavy chains, this Dync2h1 contains 4 conserved ATP-binding domains, called P-loops (Holzbaur and Vallee, 1994), as highlighted in the predicted protein sequence (Supplementary Figure S4) and in alignment with the Dync2h1 sequences



The btv^1 mutation is a small deletion that affects CG15148 but not CG5674. (A) Diagram of the region near CG15148 exon 13 encoding Dync2h1 (Dhc36D). The BG01771 transposon insertion site and the positions of primers used in B are shown. (B) PCR results with genomic DNA templates listed. The expected 2,670 bp amplicon is recovered in all genotypes shown except btv^1 . (C) Sequencing of the btv^1 genomic DNA in this region confirms a small deletion of 401 bp, in addition to a 6 bp insertion that appears to be a tandem duplication of sequences (in bold) flanking one end of the deletion. Exon sequences are shown in upper case, intron in lower case.

from several species across the ciliated taxa (Supplementary Figure S5). The sequence of P-loop 1, GPAGTGKT, is identical to that in all other dyneins. P-loops 2 and 3 show intermediate levels of conservation, while P-loop 4 shows the least similarity between organisms (Supplementary Figure S5). To examine the localization of the Btv protein, we generated a monoclonal antibody against a Btv peptide in collaboration with the Developmental Studies Hybridoma Bank. Unfortunately, this antibody showed no signal on Western blots or in tissues (data not shown).

Beethoven mutation disrupts retrograde IFT in chordotonal sensory cilia

To confirm that this Dync2h1 dynein motor performs the retrograde IFT function in *Drosophila*, we examined the morphological phenotype of sensory neurons in the auditory organ, JO. We previously showed that the kinesin II motor, including the Klp64D heavy chain and DmKAP, mediates the

anterograde IFT motor function (Sarpal et al., 2003). Loss of anterograde function causes complete failure to extend an axoneme from the JO basal bodies. With loss of retrograde motor function, we expect anterograde transport to be largely intact, resulting in partial axoneme assembly. However, retrograde transport is required for clearing the growing cilium of assembly byproducts, so we expect that as growth and assembly proceed, proteins and complexes that would normally be cleared will accumulate, leading to impaired assembly. Consistent with this, we previously reported morphological defects that include partial and variable assembly of the axoneme and abnormal swellings of the ciliary membrane (Eberl et al., 2000). Our further ultrastructural analysis (Figures 2–4) shows ciliary defects that are fully consistent with loss of retrograde IFT.

If retrograde IFT is disrupted, we should expect accumulation of IFT components in the cilium due to failure of the retrograde transport clearing function. Thus, we examined the expression and distribution of the GFP-NompB protein (Han et al., 2003), which encodes the IFT complex B protein homologous to Chlamydomonas IFT88, in btv mutants. In the mature JO, GFP-NompB normally localizes to the cilium, with most fluorescence near the ciliary tip, in the vicinity of the ciliary dilation (Figure 7A). In JO cilia of similarly staged in btv1 mutants, imaged under identical conditions, the GFP-NompB protein correctly localizes to the cilium. However, localization within the cilium is disrupted, showing excess fluorescence both in proximal cilium close to the basal bodies, as well as ectopic fluorescence distally (Figure 7B). This distal fluorescence likely represents ciliary material sloughed off in a "trail of crumbs" fashion along the length of the tubular dendritic cap, where it is left behind developmentally rather than being cleared toward the cell body by retrograde IFT motor activity. Unlike growth of unattached cilia such as Chlamydomonas flagella, the JO cilia, embraced by the dendritic cap, extend in concert with extensive developmental stretching of the scolopidium (Figure 7C). The dendritic cap forms early in antennal development (Todi et al., 2008), and in the btv mutant, developmental stretching culminates in the cilium stretching to its normal length despite failure of proper axonemal growth. Thus, finding distal fragments of cilium indicates a failure of the cilium to remain intact during scolopidium elongation, rather than excess extension of the cilium. Therefore, the delocalization of GFP-NompB in btv mutants supports a retrograde IFT transport function for the btv-encoded dynein.

Beethoven mutation de-localizes IFT140 and reduces mechanoreceptor potentials in external sensory organ dendrites

Cachero et al. (2011) reported that Dync2h1 transcripts in embryos show a "chordotonal-enriched pattern," with some additional lower level expression in es organs. To test whether btv mutant phenotypes are confined to ch organs, we examined the localization of RempA-YFP, a labelled version of the IFT140 protein (Lee et al., 2008) in btv mutant campaniform organs and bristle organs. In ch organs, we had previously shown that RempA-YFP is de-localized in btv¹ mutants, extending beyond the normal location of the ciliary tip (Lee et al., 2008). In campaniform organs of the haltere, RempA-YFP is normally confined near the proximal connecting cilium and proximal to

the distal, non-axonemal region of the dendrite, but in *btv* mutants RempA is released distally, extending to the dome and filling the blade-shaped distal tip of the dendrite (Figures 8A–C). Similarly, in *btv* mutant bristle organs of the adult abdomen, RempA colocalizes with the distal dendritic cap marker NompA, in contrast with their discrete localization patterns in the wild type (Figures 8D,E).

To test for electrophysiological effects of btv mutations on bristle organs, we recorded transepithelial potentials (TEPs) and mechanoreceptor potentials (MRPs) (Figures 9A,B) as previously described (Kernan et al., 1994). We found that, although TEPs do not differ significantly between btv mutants and control flies (Figure 9C), MRPs are reduced by about 50% in btv mutants (8.1±0.9 mV) compared to controls (17.4±1.3 mV; t-test with Welch's correction, p<0.0001) (Figure 9D). Adaptation of the MRP, (ratio of peak and end-stimulus MRP amplitudes) is the same in btv and controls (Figure 9E).

Regarding age effects on bristle organ function, although MRP amplitudes are slightly reduced in old $(15.5\pm1.7\,\mathrm{mV})$ vs. young $(20.9\pm1.7\,\mathrm{mV})$ control flies $(t\text{-test},p\!<\!0.04)$ (Supplementary Figure S6), this is not significant in btv mutants $(7.6\pm1.6\,\mathrm{mV})$ vs. $8.5\pm1.1\,\mathrm{mV}$; $t\text{-test},p\!=\!0.66$). Six out of 38 old bristles were non-responders, but these were divided between both control (3 of 21) and btv mutants (3 of 17). These data do not support accelerated degeneration in btv mutant bristles.

Discussion

The Dync2h1 encoded by btv performs IFT in chordotonal organs

Several lines of evidence support the conclusion that the btvencoded Dync2h1 carries out the retrograde IFT function. First, as in all other organisms characterized, there is only a single Dync2h1 gene in the Drosophila genome. Ciliary function for Dync2h1 is supported by studies that report btv gene expression in ciliated cells. The btv gene expression is regulated by the Rfx transcription factor (Laurençon et al., 2007), as would be expected for a central component of IFT. In that study, btv gene expression was reduced by 124 fold in dRfx mutants. By in situ hybridization, btv gene expression was seen in embryonic ch organs, and in embryonic cellsorting microarray experiments, btv gene expression showed 8-fold enrichment in cell lineages associated with the chordotonal proneural gene atonal (Cachero et al., 2011). Furthermore, the btvencoded Dync2h1 is directly regulated by the forkhead transcription factor Fd3F (Newton et al., 2012), a regulator of ciliary genes. Binding sites for these two transcription factors are identified in the promoter region of the DCH1b gene [Figure 5D, (Laurençon et al., 2007; Newton et al., 2012)].

Secondly, the profile of chordotonal defects we see in the *btv* mutant, including axonemal disruption and loss of ciliary integrity that worsens with distance from the basal bodies, is entirely consistent with loss of retrograde IFT. The defects are remarkably similar to those we documented for *rempA* mutants (Lee et al., 2008), encoding IFT140, an IFT-A particle protein that should be transported by Dync2h1 in retrograde IFT. This similarity is consistent with the idea that the Btv-mediated assembly of cilia is carried out through transport of IFT-A complexes including RempA.

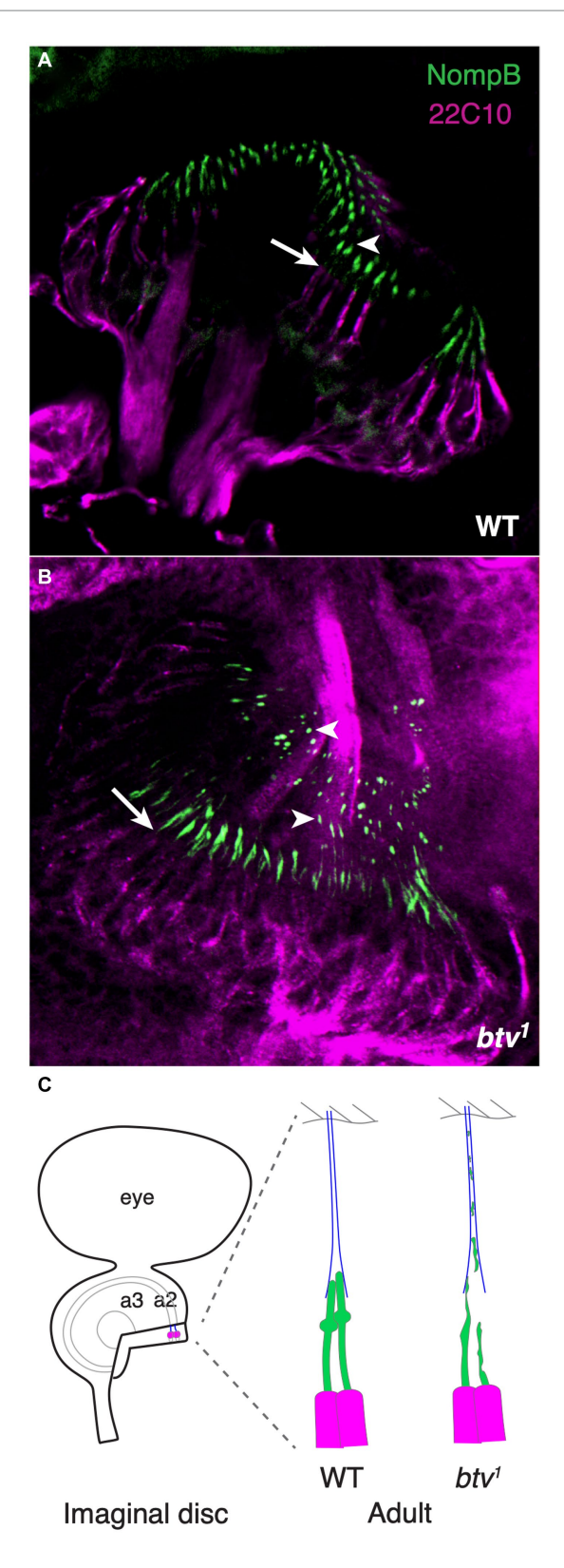


FIGURE 7

NompB is delocalized in *btv* mutant chordotonal neurons. (A) GFP-tagged NompB (green), encoding the IFT-B protein IFT88, normally localizes in the ciliated outer dendritic segment distal to the basal bodies at the end of the inner dendritic segment (arrow indicates transition from inner to outer dendritic segment) in the late pupal JO, ending at the ciliary tip (arrowhead) just distal to the ciliary dilation. Counterstain is mAb 22C10 (magenta), which stains all neurons, and labels chordotonal neurons including the inner dendritic segment, but not the cilium. (B) In JO of late pupal *btv*¹ mutants, GFP-NompB is delocalized beyond the basal bodies (arrow), with some GFP-NompB protein delocalized to regions extending along the dendritic cap (arrowheads), in some cases as far as the a2/a3 joint. (C) The schematics highlight our interpretation of the normal and mutant localization of NompB. JO development from newly specified sense organs in the imaginal disc involved extensive elongation enroute to the adult configuration, with the tubular dendritic cap (blue) maintaining the physical connection between the cilia tips and the antennal joint cuticle. Structural defects in *btv* mutant cilia results in loss of ciliary fragments, leaving a developmental "trail of crumbs".

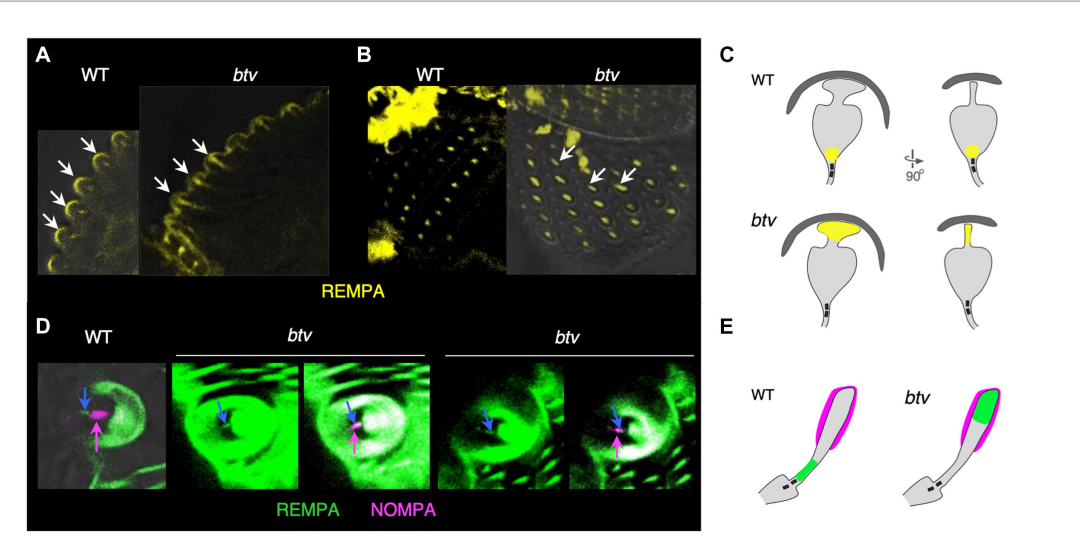


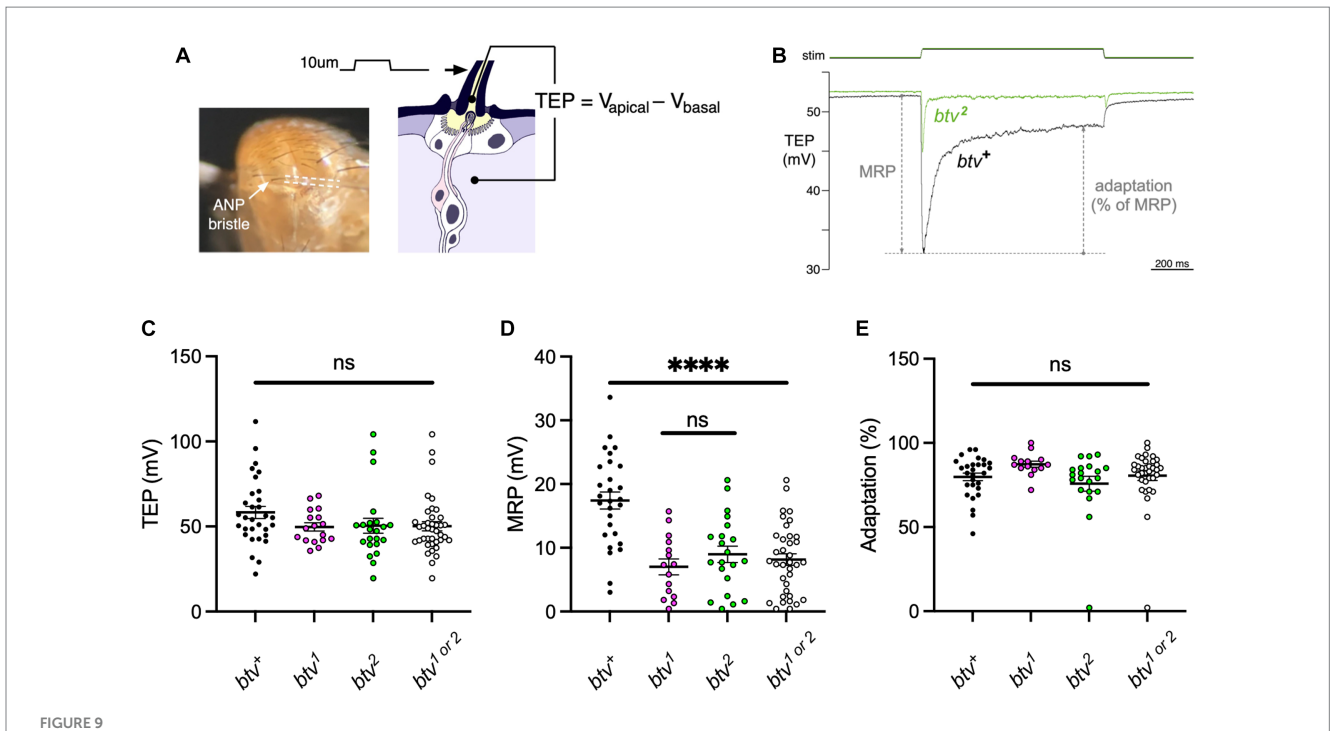
FIGURE 8

IFT140/RempA is mislocalized in *btv* mutant es organs. Transverse (A) and overhead (B) views of haltere campaniform sensilla in pharate adults expressing YFP-labelled IFT140 (RempA). Arrows in (A) indicate the apex of autofluorescent campaniform domes, highlighting in the *btv* mutant abnormal extension of IFT140 labeling beyond the connecting cilium where it is normally restricted, into the distal non-axonemal region of the dendrite. Arrows in (B) indicate elongated IFT140 staining in *btv* mutant dendrites. (C) Orthogonal sketches of the ciliary outer segments, based on Figure 1 of Sun et al. (2019). IFT140 is localized at the connecting cilium in the wild type, but is mislocalized to the blade-shaped distal tip in *btv* mutants, appearing as a line instead of a dot in the overhead view. (D) Bristle bases in the pharate adult abdomen, in which the dendritic cap that covers the distal outer segment is labelled with NompA (magenta). (E) Schematic of the outer segment, drawn after Figure 1 in Walker et al. (2000). In the wild type, IFT140 (blue arrow) localizes proximal to the dendritic cap (magenta arrow), but in *btv* mutants, the two proteins are colocalized. Two examples of mutant abdominal bristles are shown; for each, the left panel shows the RempA channel alone, while the right panel shows both IFT140/RempA and NompA channels.

Additional evidence supporting a retrograde IFT function for the Btv protein involves the mislocalization of other components in btv mutants. Here we show that NompB, encoding the IFT-B complex protein IFT88, is abnormally distributed in defective cilia of btv mutant JO. This agrees with the finding of Lee et al. (2010) that both IFT88 and the TRPN ion channel NompC are mislocalized in btv mutants. Also, in embryonic ch organs, Kwon et al. (2020) reported that the transport requirements of NompC and TRPV ion channel Iav for Dync2h1 are different, where Dync2h1 is required for both pre-ciliary trafficking and retrograde transport of NompC, primarily in the distal compartment, while Iav only requires Dync2h1 for the former. Furthermore, Lee et al. (2018) used time-lapse imaging to show that retrograde movement of GFP-NompB is absent in btv1 mutants. NompC is normally localized only to the distal ciliary segment, beyond the ciliary dilation, and NompB and Iav are delimited to the proximal segment, but btv mutants lack a ciliary dilation and lose the sequestered localization of these proteins. Furthermore, we previously showed that RempA, normally restricted to the ciliary dilation by the adult stage, and the Iav, normally delimited to the proximal ciliary segment, are also mislocalized in btv mutants (Lee et al., 2008). Mutation of btv also results in redistribution of the Eys/Spam extracellular matrix protein that is normally deposited into the scolopale space, and that provides protection against desiccation at high temperature conditions (Cook et al., 2008). This protein is normally distributed into a major mid-scolopale space region and a minor proximal region immediately adjacent to the inner dendritic segment; in btv mutants this collapses into a single larger proximal cluster (Lee et al., 2008). It is not clear whether this redistribution arises from loss of a positioning cue provided by the sensory cilium, or whether distal ciliary bloating or membrane leakage forces the scolopale space material more proximally. On the other hand, the *Drosophila* Tubby-like protein dTulp is not mislocalized in *btv* mutants (Park et al., 2013). In summary, in the current study we show detailed ultrastructural evidence of the *btv* mutant, along with mislocalization of ciliary proteins in the *btv* mutant background, including NompB and RempA. Overall, the *btv* mutant morphological defects combined with the spectrum of mislocalized proteins demonstrate clearly that Dync2h1 encoded by *btv* is centrally involved in retrograde IFT in ch organs.

Functional role of Dync2h1 encoded by btv in external sensory organs

Our finding of altered relative distribution of RempA-YFP and NompA in btv mutants is consistent with our finding of functional defects as reflected by reduced MRPs. Nevertheless, the functional consequences of btv dysfunction in es organs is relatively mild compared to those in ch organs. In es organs, the axonemal segment of the cilium is very short, while the tubular bundle of the distal dendrite is non-axonemal. In contrast to the defective ch cilia tips, the distinctive tip shape of campaniform sensilla is retained, but accumulates RempA (Figure 8). If Dync2h1 requires axonemal structure as a substrate to move cargo, then it may be possible for some cargoes to diffuse along such a short distance sufficiently well to move into the dendrite. Thus, despite de-localization of RempA and NompA, assembly of sensory structures in es organs is sufficient to provide some mechanosensory function. Even in ch organs, where the ciliary segments are relatively long, some residual sensory function is maintained in btv null mutants. Alternatively, it is possible that in es organs, the Dync2h1 function is not specifically



btv mutations affect mechanoreceptor potentials but not transepithelial potentials in bristle organs. (A) Recording bristle transepithelial potentials. The decapitated fly is mounted on a chlorided silver pin, which serves as a basal reference electrode. The anterior notopleural (ANP) bristle is cut to half its length, giving access to the lymph in apical extracellular space, and a saline-filled glass microelectrode (outlined by dashed lines), attached to a piezoelectric positioner, is placed over the cut end. The TEP, an apical-positive potential maintained by the ion pumping activity of bristle support cells, is recorded as the voltage difference between the apical and basal electrodes. (B) Representative mechanoreceptor potentials (MRP) recorded from btv⁺ and btv² flies; each trace is an average of 5 trials. The MRP value is the maximal change in TEP immediately following a 10 µm step deflection of the microelectrode and bristle; adaptation is calculated as the % reduction in this change by the end of the 1s stimulus. C-E: btv mutants show a significant reduction in MRP amplitudes, but no significant change in resting TEP or in adaptation. (C) TEP measured in btv⁺, btv⁻, and btv². Each dot represents the TEP of a single bristle. Horizontal bars indicate means, error bars indicate SEM. The point scatter bar on the right includes the data from both btv alleles tested (btv¹ and btv²). TEP is unaffected in btv mutants. Symbols as in (C). (E) Adaptation is unaffected in btv mutants. Symbols as in (C).

IFT per se, but a related transport function for certain cargo proteins, including RempA. Dync2h1 does not appear to have a role in establishing the TEP, suggesting that the ion transport mechanisms to establish and maintain the receptor lymph properties do not depend on this dynein motor. Although some forms of mechanosensory adaptation are motor-driven, loss of Dync2h1 does not affect the MRP adaptation, suggesting that adaptation does not require this dynein.

Use of IFT dynein in diverse cilia and flagella

Until recently, ciliary assembly was thought to be universally dependent upon IFT. Consistent with this, we find that retrograde IFT function mediated by Dync2h1 in *Drosophila* is essential for normal ciliary assembly in ch organ sensory cilia, including JO. In es organs, which have short ciliary segments, the Dync2h1 has a more modest requirement. Dync2h1 is dispensable in sperm flagella: *btv* mutants are male-fertile (Eberl et al., 2000). Other exceptions to IFT-dependence have been found. This supports the idea that in *Drosophila*, contrary to many other taxa, assembly of the sperm flagellum axoneme employs an IFT-independent mechanism (Han et al., 2003; Sarpal et al., 2003; Lee et al., 2008). While the Rfx

transcription factor is transiently expressed during spermatid development (Vandaele et al., 2001), there is no evidence available that Rfx activates ciliary genes for spermiogenesis. Furthermore, in a survey of ciliary motility machinery, it was found that a surprising number of axonemal components are encoded by separate genes in sperm compared to mechanosensory cilia (Zur Lage et al., 2019). While IFT is highly conserved in *Drosophila*, it is activated only in sensory cilia, not in the male germline. In mammals, however, IFT is essential for spermiogenesis, though not for maintenance of sperm tail flagella (San Agustin et al., 2015).

In *Tetrahymena*, Dync2h1 (*dhc-2*) appears to be dispensable for ciliary integrity, though it regulates cilia length such that in mutants, ciliary length is variable and cilia are fewer in number (Rajagopalan et al., 2009). Furthermore, in this ciliate, IFT122A, an IFT-A complex protein, participates in retrograde trafficking of IFT88 and IFT172 proteins; these proteins accumulate in the cilia but ciliary assembly is not significantly disrupted (Tsao and Gorovsky, 2008). On the other hand, Dync2h1 phenotypes in *Chlamydomonas* (Pazour et al., 1999) and in *Caenorhabditis* (Signor et al., 1999; Wicks et al., 2000) are more severe, while the phenotypes we see in *Drosophila* ch organs are intermediate, allowing a small amount of residual sensory function. Thus, there is both taxonomic and cell type variation in the degree to which ciliary assembly can proceed with compromised retrograde IFT dynein function.

Residual hearing function in *btv* mutants decreases with age through non-apoptotic degeneration

Our finding that btv mutants, while suffering strong hearing loss, are not completely deaf in contrast to other auditory mutants such as tilB (Kavlie et al., 2010), iav and nan (Kim et al., 2003; Gong et al., 2004) and the kinesin II mutants klp64D and DmKAP (Sarpal et al., 2003). This allowed us to test for progressive hearing loss, leading to our finding that by 30 days of age, btv mutant flies have a significant reduction in auditory capacity, evident primarily in the reduced fraction of flies retaining any residual auditory response. Morphologically, we see strong degeneration in many mutant cilia. However, we see no evidence that the sensory neurons die during this interval, and the lack of TUNEL labeling is consistent with degeneration and resorption of material only in the ciliary compartment.

Even in wild-type flies we see some hearing loss with age, consistent with other studies (Keder et al., 2020). We also see morphological changes with age that likely reflect the fact that, as in vertebrates, the auditory periphery encounters strong metabolic challenges. These changes include the deposition of excess membranes and increasing signs of putative disruption of ionic homeostasis. The morphological changes correlate with age-dependent reductions in hearing, but at present we cannot determine whether there is a causal relationship between these factors. The answer to this question must await further study, and may require the ability to record from single auditory neurons.

Data availability statement

The datasets presented in this study can be found in online repositories. The names of the repository/repositories and accession number (s) can be found in the article/Supplementary material.

Ethics statement

The manuscript presents research on animals that do not require ethical approval for their study.

Author contributions

YS: Conceptualization, Data curation, Formal analysis, Investigation, Methodology, Visualization, Writing – original draft, Writing – review & editing. JJ: Conceptualization, Data curation, Formal analysis, Investigation, Methodology, Visualization, Writing – review & editing. ES-L: Conceptualization, Data curation, Formal analysis, Investigation, Methodology, Visualization, Writing – review & editing. EL: Conceptualization, Data curation, Formal analysis, Investigation,

Methodology, Visualization, Writing – review & editing. MK: Conceptualization, Data curation, Formal analysis, Funding acquisition, Investigation, Methodology, Project administration, Supervision, Visualization, Writing – original draft, Writing – review & editing. DE: Conceptualization, Data curation, Formal analysis, Funding acquisition, Investigation, Methodology, Project administration, Supervision, Visualization, Writing – original draft, Writing – review & editing.

Funding

This work was supported by NIH NIDCD grants R01 DC004848 (to DE), P30 DC010362 (to Steven Green) and R01 DC002780 (to MK), and NSF grant 2037828 (to Alan Kay, DE and Zahra Aminzare).

Acknowledgments

We are grateful to Jason Caldwell, Brian McNeer, Matthew Miller, Jill Pottratz, Mary Bryant, Adam Schlichte, Merav Tauber, and Eran Tauber for contributions during early stages of this work, and to all members of the Eberl and Kernan labs for productive discussions. We thank the Developmental Studies Hybridoma Bank at the University of Iowa for antibodies. We appreciate the Carver Center for Genomics, and the Carver Center for Imaging in the Biology Department for facilities and support. The Central Microscopy Research Facility at the University of Iowa provided electron microscope access.

Conflict of interest

The authors declare that the research was conducted in the absence of any commercial or financial relationships that could be construed as a potential conflict of interest.

Publisher's note

All claims expressed in this article are solely those of the authors and do not necessarily represent those of their affiliated organizations, or those of the publisher, the editors and the reviewers. Any product that may be evaluated in this article, or claim that may be made by its manufacturer, is not guaranteed or endorsed by the publisher.

Supplementary material

The Supplementary material for this article can be found online at: https://www.frontiersin.org/articles/10.3389/fnmol.2023.1263411/full#supplementary-material

References

Armstrong, J. D., Texada, M. J., Munjaal, R., Baker, D. A., and Beckingham, K. M. (2006). Gravitaxis in Drosophila melanogaster: a forward genetic screen. *Genes Brain Behav.* 5, 222–239. doi: 10.1111/j.1601-183X.2005.00154.x

Bellen, H. J., Levis, R. W., Liao, G., He, Y., Carlson, J. W., Tsang, G., et al. (2004). The Bdgp gene disruption project: single transposon insertions associated with 40% of Drosophila genes. *Genetics* 167, 761–781. doi: 10.1534/genetics.104.026427

Braschi, B., Omran, H., Witman, G. B., Pazour, G. J., Pfister, K. K., Bruford, E. A., et al. (2022). Consensus nomenclature for dyneins and associated assembly factors. *J. Cell Biol.* 221:e202109014. doi: 10.1083/jcb.202109014

Cachero, S., Simpson, T. I., Zur Lage, P. I., Ma, L., Newton, F. G., Holohan, E. E., et al. (2011). The gene regulatory cascade linking proneural specification with differentiation in Drosophila sensory neurons. *PLoS Biol.* 9:e1000568. doi: 10.1371/journal.pbio.1000568

- Caldwell, J. C., Fineberg, S. K., and Eberl, D. F. (2007). Reduced ocelli encodes the leucine rich repeat protein pray for elves in Drosophila melanogaster. *Fly* 1, 146–152. doi: 10.4161/fly.4562
- Caldwell, J. C., Miller, M. M., Wing, S., Soll, D. R., and Eberl, D. F. (2003). Dynamic analysis of larval locomotion in Drosophila chordotonal organ mutants. *Proc. Natl. Acad. Sci. U. S. A.* 100, 16053–16058. doi: 10.1073/pnas.2535546100
- Chen, B., Chu, T., Harms, E., Gergen, J. P., and Strickland, S. (1998). Mapping of Drosophila mutations using site-specific male recombination. *Genetics* 149, 157–163. doi: 10.1093/genetics/149.1.157
- Chien, A., Shih, S. M., Bower, R., Tritschler, D., Porter, M. E., and Yildiz, A. (2017). Dynamics of the IFT machinery at the ciliary tip. *elife* 6:e28606. doi: 10.7554/eLife.28606
- Chung, Y. D., Zhu, J., Han, Y.-G., and Kernan, M. J. (2001). nompA encodes a PNS-specific, Zp domain protein required to connect mechanosensory dendrites to sensory structures. *Neuron* 29, 415–428. doi: 10.1016/S0896-6273(01)00215-X
- Cole, D. G., Diener, D. R., Himelblau, A. L., Beech, P. L., Fuster, J. C., and Rosenbaum, J. L. (1998). Chlamydomonas kinesin-ii-dependent intraflagellar transport (Ift): Ift particles contain proteins required for ciliary assembly in Caenorhabditis elegans sensory neurons. *J. Cell Biol.* 141, 993–1008. doi: 10.1083/jcb.141.4.993
- Comeron, J. M., Reed, J., Christie, M., Jacobs, J. S., Dierdorff, J., Eberl, D. F., et al. (2016). A mismatch endo nuclease array-based methodology (mena) for identifying known Snps or novel point mutations. *Microarrays* 5:E7. doi: 10.3390/microarrays5020007
- Cook, B., Hardy, R. W., Mcconnaughey, W. B., and Zuker, C. S. (2008). Preserving cell shape under environmental stress. *Nature* 452, 361–364. doi: 10.1038/nature06603
- Criswell, P. S., and Asai, D. J. (1998). Evidence for four cytoplasmic dynein heavy chain isoforms in rat testis. *Mol. Biol. Cell* 9, 237–247. doi: 10.1091/mbc.9.2.237
- Criswell, P. S., Ostrowski, L. E., and Asai, D. J. (1996). A novel cytoplasmic dynein heavy chain: expression of Dhc 1b in mammalian ciliated epithelial cells. *J. Cell Sci.* 109, 1891–1898. doi: 10.1242/jcs.109.7.1891
- Dagoneau, N., Goulet, M., Genevieve, D., Sznajer, Y., Martinovic, J., Smithson, S., et al. (2009). Dync 2H1 mutations cause asphyxiating thoracic dystrophy and short ribpolydactyly syndrome, type iii. *Am. J. Hum. Genet.* 84, 706–711. doi: 10.1016/j. ajhg.2009.04.016
- Durand, B., Vandaele, C., Spencer, D., Pantalacci, S., and Couble, P. (2000). Cloning and characterization of drfx, the Drosophila member of the Rfx family of transcription factors. *Gene* 246, 285–293. doi: 10.1016/S0378-1119(00)00093-7
- Eberl, D. F., Duyk, G. M., and Perrimon, N. (1997). A genetic screen for mutations that disrupt an auditory response in Drosophila melanogaster. *Proc. Natl. Acad. Sci. U. S. A.* 94, 14837–14842. doi: 10.1073/pnas.94.26.14837
- Eberl, D. F., Hardy, R. W., and Kernan, M. (2000). Genetically similar transduction mechanisms for touch and hearing in Drosophila. *J. Neurosci.* 20, 5981–5988. doi: 10.1523/JNEUROSCI.20-16-05981.2000
- Eberl, D. F., and Kernan, M. J. (2011). Recording sound-evoked potentials from the Drosophila antennal nerve. *Cold Spring Harb. Protoc.* 2011:prot5576. doi: 10.1101/pdb. prot5576
- Fabre, C. C., Hedwig, B., Conduit, G., Lawrence, P. A., Goodwin, S. F., and Casal, J. (2012). Substrate-borne vibratory communication during courtship in Drosophila melanogaster. *Curr. Biol.* 22, 2180–2185. doi: 10.1016/j.cub.2012.09.042
- Gong, Z., Son, W., Chung, Y. D., Kim, J., Shin, D. W., Mcclung, C. A., et al. (2004). Two interdependent Trpv channel subunits, inactive and Nanchung, mediate hearing in Drosophila. *J. Neurosci.* 24, 9059–9066. doi: 10.1523/JNEUROSCI.1645-04.2004
- Gramates, L. S., Agapite, J., Attrill, H., Calvi, B. R., Crosby, M. A., Dos Santos, G., et al. (2022). Flybase: a guided tour of highlighted features. Genetics 220:iyac035. doi: 10.1093/genetics/iyac035
- Han, Y.-G., Kwok, B. H., and Kernan, M. J. (2003). Intraflagellar transport is required in Drosophila to differentiate sensory cilia but not sperm. *Curr. Biol.* 13, 1679–1686. doi: 10.1016/j.cub.2003.08.034
- Hesketh, S. J., Mukhopadhyay, A. G., Nakamura, D., Toropova, K., and Roberts, A. J. (2022). Ift-a structure reveals carriages for membrane protein transport into cilia. *Cells* 185:e16. doi: 10.1016/j.cell.2022.11.010
- Hildebrandt, F., Benzing, T., and Katsanis, N. (2011). Ciliopathies. N. Engl. J. Med. 364, 1533–1543. doi: 10.1056/NEJMra1010172
- Holzbaur, E. L., and Vallee, R. B. (1994). Dyneins: molecular structure and cellular function. *Annu. Rev. Cell Biol.* 10, 339–372. doi: 10.1146/annurev.cb.10.110194.002011
- Ishikawa, H., and Marshall, W. F. (2017). Intraflagellar transport and ciliary dynamics. Cold Spring Harb. Perspect. Biol. 9:a021998. doi: 10.1101/cshperspect.a021998

Jordan, M. A., Diener, D. R., Stepanek, L., and Pigino, G. (2018). The cryo-Em structure of intraflagellar transport trains reveals how dynein is inactivated to ensure unidirectional anterograde movement in cilia. *Nat. Cell Biol.* 20, 1250–1255. doi: 10.1038/s41556-018-0213-1

- $\label{eq:continuous} Jordan, M. A., and Pigino, G. (2021). The structural basis of intraflagellar transport at a glance. \textit{J. Cell Sci.} 134:jcs247163. doi: 10.1242/jcs.247163$
- Kamikouchi, A., Inagaki, H. K., Effertz, T., Hendrich, O., Fiala, A., Göpfert, M. C., et al. (2009). The neural basis of Drosophila gravity-sensing and hearing. *Nature* 458, 165–171. doi: 10.1038/nature07810
- Kavlie, R. G., Kernan, M. J., and Eberl, D. F. (2010). Hearing in Drosophila requires Til B, a conserved protein associated with ciliary motility. *Genetics* 185, 177–188. doi: 10.1534/genetics.110.114009
- Keder, A., Tardieu, C., Malong, L., Filia, A., Kashkenbayeva, A., Newton, F., et al. (2020). Homeostatic maintenance and age-related functional decline in the Drosophila ear. *Sci. Rep.* 10:7431. doi: 10.1038/s41598-020-64498-z
- Kernan, M., Cowan, D., and Zuker, C. (1994). Genetic dissection of mechanosensory transduction: mechanoreception-defective mutations of Drosophila. *Neuron* 12, 1195–1206. doi: 10.1016/0896-6273(94)90437-5
- Kim, J., Chung, Y. D., Park, D.-Y., Choi, S., Shin, D. W., Soh, H., et al. (2003). A Trpv family ion channel required for hearing in Drosophila. *Nature* 424, 81–84. doi: 10.1038/nature01733
- Kozminski, K. G., Johnson, K. A., Forscher, P., and Rosenbaum, J. L. (1993). A motility on the eukaryotic flagellum unrelated to flagellar beating. *Proc. Natl. Acad. Sci. U. S. A.* 90, 5519–5523. doi: 10.1073/pnas.90.12.5519
- Kwon, Y., Lee, J., and Chung, Y. D. (2020). Sub-ciliary segregation of two Drosophila transient receptor potential channels begins at the initial stage of their pre-ciliary trafficking. *Mol. Cells* 43, 1002–1010. doi: 10.14348/molcells.2020.0205
- Kwon, Y., Shen, W. L., Shim, H.-S., and Montell, C. (2010). Fine thermotactic discrimination between the optimal and slightly cooler temperatures via a Trpv channel in chordotonal neurons. *J. Neurosci.* 30, 10465–10471. doi: 10.1523/INEUROSCI.1631-10.2010
- Lacey, S. E., Foster, H. E., and Pigino, G. (2023). The molecular structure of IFT-A and IFT-B in anterograde intraflagellar transport trains. *Nat. Struct. Mol. Biol.* 30, 584–593. doi: 10.1038/s41594-022-00905-5
- Laurençon, A., Dubruille, R., Efimenko, E., Grenier, G., Bissett, R., Cortier, E., et al. (2007). Identification of novel regulatory factor X (Rfx) target genes by comparative genomics in Drosophila species. *Genome Biol.* 8:R195. doi: 10.1186/gb-2007-8-9-r195
- Lechtreck, K. (2022). Cargo adapters expand the transport range of intraflagellar transport. J. Cell Sci. 135;jcs260408, doi: 10.1242/jcs.260408
- Lee, J., Moon, S., Cha, Y., and Chung, Y. D. (2010). Drosophila Trpn (=Nompc) channel localizes to the distal end of mechanosensory cilia. *Publ. Library Sci. One* 5:e11012. doi: 10.1371/journal.pone.0011012
- Lee, N., Park, J., Bae, Y. C., Lee, J. H., Kim, C. H., and Moon, S. J. (2018). Time-lapse live-cell imaging reveals dual function of Oseg 4, Drosophila Wdr 35, in ciliary protein trafficking. *Mol. Cells* 41, 676–683. doi: 10.14348/molcells.2018.0179
- Lee, E., Sivan-Loukianova, E., Eberl, D. F., and Kernan, M. J. (2008). An IFT-a protein is required to delimit functionally distinct zones in mechanosensory cilia. *Curr. Biol.* 18, 1899–1906. doi: 10.1016/j.cub.2008.11.020
- Li, B., Li, S., Zheng, H., and Yan, Z. (2021). Nanchung and inactive define pore properties of the native auditory transduction channel in Drosophila. *PNAS Nexus* 118:e2106459118. doi: 10.1073/pnas.2106459118
- Liu, L., Yermolaieva, O., Johnson, W. A., Abboud, F. M., and Welsh, M. J. (2003). Identification and function of thermosensory neurons in Drosophila larvae. *Nat. Neurosci.* 6, 267–273. doi: 10.1038/nn1009
- Mamiya, A., Gurung, P., and Tuthill, J. C. (2018). Neural coding of leg proprioception in Drosophila. Neuron 100:e6. doi: 10.1016/j.neuron.2018.09.009
- Mancebo, R., Zhou, X., Shillinglaw, W., Henzel, W., and Macdonald, P. M. (2001). BSF binds specifically to the bicoid mrna 3' untranslated region and contributes to stabilization of bicoid MRNA. *Mol. Cell. Biol.* 21, 3462–3471. doi: 10.1128/MCB.21.10.3462-3471.2001
- Marszalek, J. R., Liu, X., Roberts, E. A., Chui, D., Marth, J. D., Williams, D. S., et al. (2000). Genetic evidence for selective transport of opsin and arrestin by kinesin-II in mammalian photoreceptors. *Cells* 102, 175–187. doi: 10.1016/S0092-8674(00)00023-4
- Meleppattu, S., Zhou, H., Dai, J., Gui, M., and Brown, A. (2022). Mechanism of IFT-a polymerization into trains for ciliary transport. *Cells* 185:e12. doi: 10.1016/j. cell.2022.11.033
- Merrill, A. E., Merriman, B., Farrington-Rock, C., Camacho, N., Sebald, E. T., Funari, V. A., et al. (2009). Ciliary abnormalities due to defects in the retrograde transport protein Dync 2H1 in short-rib polydactyly syndrome. *Am. J. Hum. Genet.* 84, 542–549. doi: 10.1016/j.ajhg.2009.03.015
- Mikami, A., Tynan, S. H., Hama, T., Luby-Phelps, K., Saito, T., Crandall, J. E., et al. (2002). Molecular structure of cytoplasmic dynein 2 and its distribution in neuronal and ciliated cells. *J. Cell Sci.* 115, 4801–4808. doi: 10.1242/jcs.00168
- Newton, F. G., Zur Lage, P. I., Karak, S., Moore, D. J., Göpfert, M. C., and Jarman, A. P. (2012). Forkhead transcription factor Fd3F cooperates with RFX to regulate a gene

expression program for mechanosensory cilia specialization. $Dev.\ Cell\ 22,\ 1221-1233.$ doi: 10.1016/j.devcel.2012.05.010

Ojeda Naharros, I., and Nachury, M. V. (2022). Shedding of ciliary vesicles at a glance. *J. Cell Sci.* 135:jcs246553. doi: 10.1242/jcs.246553

Park, J., Lee, J., Shim, J., Han, W., Lee, J., Bae, Y. C., et al. (2013). Dtulp, the Drosophila melanogaster homolog of tubby, regulates transient receptor potential channel localization in cilia. *Publ. Library Sci. Gen.* 9:e1003814. doi: 10.1371/journal.pgen.1003814

Parker, J. D. K., and Quarmby, L. M. (2003). Chlamydomonas fla mutants reveal a link between deflagellation and intraflagellar transport. *BMC Cell Biol.* 4:11. doi: 10.1186/1471-2121-4-11

Pazour, G. J., Baker, S. A., Deane, J. A., Cole, D. G., Dickert, B. L., Rosenbaum, J. L., et al. (2002). The intraflagellar transport protein, IFT 88, is essential for vertebrate photoreceptor assembly and maintenance. *J. Cell Biol.* 157, 103–114. doi: 10.1083/jcb.200107108

Pazour, G. J., Dickert, B. L., and Witman, G. B. (1999). The Dhc 1b (Dhc 2) isoform of cytoplasmic dynein is required for flagellar assembly. *J. Cell Biol.* 144, 473–481. doi: 10.1083/jcb.144.3.473

Petriman, N. A., Loureiro-Lopéz, M., Taschner, M., Zacharia, N. K., Georgieva, M. M., Boegholm, N., et al. (2022). Biochemically validated structural model of the 15-subunit intraflagellar transport complex IFT-B. *EMBO J.* 41:e112440. doi: 10.15252/embi.2022112440

Pigino, G. (2021). Intraflagellar transport. Curr. Biol. 31, R530–R536. doi: 10.1016/j.cub.2021.03.081

Rajagopalan, V., Subramaniam, A., Wilkes, D. E., Pennock, D. G., and Asai, D. J. (2009). Dynein-2 affects the regulation of ciliary length but is not required for ciliogenesis in Tetrahymena thermophila. *Mol. Biol. Cell* 20, 708–720. doi: 10.1091/mbc.

Rosenbaum, J. L., and Witman, G. B. (2002). Intraflagellar transport. *Nat. Rev. Mol. Cell Biol.* 3, 813–825. doi: 10.1038/nrm952

San Agustin, J. T., Pazour, G. J., and Witman, G. B. (2015). Intraflagellar transport is essential for mammalian spermiogenesis but is absent in mature sperm. *Mol. Biol. Cell* 26, 4358–4372. doi: 10.1091/mbc.E15-08-0578

Sarpal, R., Todi, S. V., Sivan-Loukianova, E., Shirolikar, S., Subramanian, N., Raff, E. C., et al. (2003). Drosophila KAP interacts with the kinesin II motor subunit KLP 64D to assemble chordotonal sensory cilia, but not sperm tails. *Curr. Biol.* 13, 1687–1696. doi: 10.1016/j.cub.2003.09.025

Sehadova, H., Glaser, F. T., Gentile, C., Simoni, A., Giesecke, A., Albert, J. T., et al. (2009). Temperature entrainment of Drosophila's circadian clock involves the gene nocte and signaling from peripheral sensory tissues to the brain. *Neuron* 64, 251–266. doi: 10.1016/j.neuron.2009.09.026

Sharma, N., Berbari, N. F., and Yoder, B. K. (2008). Chapter 13 ciliary dysfunction in developmental abnormalities and diseases. K. Y. Bradley (Ed.) *Current topics in developmental biology*. Academic Press. 85, 371–427. doi: 10.1016/S0070-2153(08)00813-2

Signor, D., Wedaman, K. P., Orozco, J. T., Dwyer, N. D., Bargmann, C. I., Rose, L. S., et al. (1999). Role of a class Dhc 1b dynein in retrograde transport of IFT motors and IFT raft particles along cilia, but not dendrites, in chemosensory neurons of living Caenorhabditis elegans. *J. Cell Biol.* 147, 519–530. doi: 10.1083/jcb.147.3.519

Spradling, A. C., Stern, D., Beaton, A., Rhem, E. J., Laverty, T., Mozden, N., et al. (1999). The Berkeley Drosophila genome project gene disruption project: single P-element insertions mutating 25% of vital Drosophila genes. *Genetics* 153, 135–177. doi: 10.1093/genetics/153.1.135

Stepanek, L., and Pigino, G. (2016). Microtubule doublets are double-track railways for intraflagellar transport trains. Science 352, 721–724. doi: 10.1126/science.aaf4594

Sun, L., Gao, Y., He, J., Cui, L., Meissner, J., Verbavatz, J. M., et al. (2019). Ultrastructural organization of Nomp C in the mechanoreceptive organelle of Drosophila campaniform mechanoreceptors. *Proc. Natl. Acad. Sci. U. S. A.* 116, 7343–7352. doi: 10.1073/pnas.1819371116

Sun, Y., Liu, L., Ben-Shahar, Y., Jacobs, J. S., Eberl, D. F., and Welsh, M. J. (2009). TRPA channels distinguish gravity sensing from hearing in Johnston's organ. *Proc. Natl. Acad. Sci. U. S. A.* 106, 13606–13611. doi: 10.1073/pnas.0906377106

Tauber, E., and Eberl, D. F. (2001). Song production in auditory mutants of Drosophila: the role of sensory feedback. *J. Comp. Physiol. A.* 187, 341–348. doi: 10.1007/s003590100206

Thibault, S. T., Singer, M. A., Miyazaki, W. Y., Milash, B., Dompe, N. A., Singh, C. M., et al. (2004). A complementary transposon tool kit for Drosophila melanogaster using P and piggy bac. *Nat. Genet.* 36, 283–287. doi: 10.1038/ng1314

Todi, S. V., Sivan-Loukianova, E., Jacobs, J. S., Kiehart, D. P., and Eberl, D. F. (2008). Myosin VIIa, important for human auditory function, is necessary for Drosophila auditory organ development. *Publ. Library Sci. One* 3:e2115. doi: 10.1371/journal.pone.0002115

Tsao, C.-C., and Gorovsky, M. A. (2008). Tetrahymena IFT 122A is not essential for cilia assembly but plays a role in returning IFT proteins from the ciliary tip to the cell body. *J. Cell Sci.* 121, 428–436. doi: 10.1242/jcs.015826

Vandaele, C., Coulon-Bublex, M., Couble, P., and Durand, B. (2001). Drosophila regulatory factor X is an embryonic type I sensory neuron marker also expressed in spermatids and in the brain of Drosophila. *Mech. Dev.* 103, 159–162. doi: 10.1016/S0925-4773(01)00340-9

Vuolo, L., Stevenson, N. L., Mukhopadhyay, A. G., Roberts, A. J., and Stephens, D. J. (2020). Cytoplasmic dynein-2 at a glance. *J. Cell Sci.* 133:jcs240614. doi: 10.1242/jcs.240614

Walker, R. G., Willingham, A. T., and Zuker, C. S. (2000). A Drosophila mechanosensory transduction channel. *Science* 287, 2229–2234. doi: 10.1126/science.287.5461.2229

Wicks, S. R., De Vries, C. J., Van Luenen, H. G. A. M., and Plasterk, R. H. A. (2000). Che-3, a cytosolic dynein heavy chain, is required for sensory cilia structure and function in Caenorhabditis elegans. *Dev. Biol.* 221, 295–307. doi: 10.1006/dbio.2000.9686

Yorozu, S., Wong, A., Fischer, B. J., Dankert, H., Kernan, M. J., Kamikouchi, A., et al. (2009). Distinct sensory representations of wind and near-field sound in the Drosophila brain. *Nature* 458, 201–205. doi: 10.1038/nature07843

Zhang, W., Yan, Z., Jan, L. Y., and Jan, Y. N. (2013). Sound response mediated by the TRP channels Nompc, Nanchung, and inactive in chordotonal organs of Drosophila larvae. *Proc. Natl. Acad. Sci. U. S. A.* 110, 13612–13617. doi: 10.1073/pnas.1312477110

Zur Lage, P., Newton, F. G., and Jarman, A. P. (2019). Survey of the ciliary motility machinery of Drosophila sperm and ciliated mechanosensory neurons reveals unexpected cell-type specific variations: a model for motile ciliopathies. *Front. Genet.* 10:24. doi: 10.3389/fgene.2019.00024

Sharma et al. (2023) "The retrograde IFT dynein is required for normal function of diverse mechanosensory cilia in *Drosophila*". Frontiers in Molecular Neuroscience.

SUPPLEMENTARY MATERIAL

Genetic analysis of btv alleles

1. htv^{l}

As described in the main text, we isolated btv^I (originally called btv^{5PI}) in a mutagenesis screen (EberlDuyk and Perrimon, 1997) for mutants with a reduced response to courtship song. This mutant was induced with ethyl methanesulfonate (EMS), which usually generates single nucleotide mutations, with small deletions induced an order of magnitude less frequently.

The btv¹ mutation was mapped to the 36E1-3 polytene chromosome region based on failure to complement two deficiency chromosomes, Df(2L)TW119 and Df(2L)TW201 (EberlHardy and Kernan, 2000), making N-cadherin (CadN) the left limit and reduced ocelli (rdo) the right limit (Fig. 5, Table 1) based on breakpoints and complementation. To refine the btv map position, we used P-induced male recombination (PIMR) (Chen et al., 1998) of btv^{I} relative to a P-element insertion in the vicinity, KG08320 (Fig. 5B). Twelve recombinants for flanking markers Sp and pr were recovered (Table S1). The btv^{I} lesion maps unequivocally to the right of KG08320, as all flanking marker exchanges aligned perfectly with the btv phenotype. One Sp^+pr recombinant, designated P2, had Minute bristles, suggesting a large deletion to the nearby M(2)36F locus to the right. Complementation tests confirmed that btv, the male sterile locus, rdo and M(2)36F are all deleted in P2, again consistent with btv mapping to the right of KG08320. This provides a left boundary for btv and rules out the CadN2 candidate (Fig. 5B). Two Pelement inserts (KG03741 and KG05889, not shown) into the rdo gene (CaldwellFineberg and Eberl, 2007) provide a right boundary because Df(2L)B11 (Fig. 5) is btv⁺ but rdo, while Df(2L)M18 is btv⁻ and rdo⁺, indicating that btv is entirely to the left of the rdo locus. Thus, among annotated genes, the candidates for btv are limited to Dync2h1 and its anti-parallel overlapping gene CG5674, as well as four small predicted genes between *Dync2h1* and *rdo* (Fig. 5B,C).

2. Transposon insertions: btv^{k07109} , $btv^{BG01771}$, btv^{f06878} , btv^{f06884}

Several transposon insertions became available through insertional mutagenesis projects. A Pelement chromosome, k07109, (Spradling et al., 1999, Török et al., 1993), contains two P{lacW} insertions, one at polytene position 25F and another at 36E, as determined by polytene chromosome in situ hybridization (Spradling et al., 1999). This chromosome failed to complement the hearing defect in btv^{l} and all deficiencies in Fig. 5A that uncover btv^{l} . We recovered a recombinant, k07109b, that removed the 25F $P\{lacW\}$ insertion, but retained the btv lesion. This allele is also called btv^2 (Table 1; Caldwell et al., 2003). This chromosome was white-eved, suggesting that the remaining P{lacW} insertion in 36E may be incomplete, consistent with another report (Mancebo et al., 2001). Nevertheless, plasmid rescue products recovered with flanking genomic DNA confirmed that the plasmid sequences in k07109b were still intact; this is consistent with the reported chromosome in situ hybridization results with plasmid sequences as probe. The flanking sequences (not shown), though consistent with a 36E location, corresponded to the fasciclin III gene, located several genes proximal to the btv region (but also not in the nearby bicoid stability factor (bsf) gene, which is also affected in this chromosome (Mancebo et al., 2001)). Thus, the btv^{k07109} lesion potentially arose as a "hit-and-run" mutation during the dysgenic mobilization event, without leaving a molecular tag in the btv gene. We identified the lesion in the btv gene through Mismatch Endonuclease Arrays (MENA) (Comeron et al., 2016), as a single nucleotide deletion in exon 22 resulting in a frameshift that introduces an early stop codon (Comeron et al., 2016). This position is in the middle of a large intron in the overlapping gene CG5674 on the opposite strand, and therefore unlikely to affect its function (Fig. 5C).

Another *P*-element, *BG01771*, is inserted into the *Dync2h1* intron separating exons 13 and 14 (Fig. 5C). This *P*-element construct contains a promoter-less Gal4 sequence with a splice acceptor, along

with a polyA-minus mini-white sequence with a splice donor (Lukacsovich et al., 2001). If the P-element inserts into a gene intron, the Gal4 would be under the control of the endogenous promoter, resulting in Gal4 expression wherever the gene is expressed. At the same time, the mini-white gene would adopt that gene's polyadenylation sequence, allowing expression of the mini-white marker. The expressed eye pigmentation confirmed the presence of the P-element in the BG01771 strain, and PCR analysis verified its insertion site. The insertion site, which lies in the predicted 3' UTR of CG5674 (1,035 bp downstream of the predicted stop codon and only 260 bases from the transcript end), is unlikely to disrupt CG5674 unless transcript stability is affected. Conversely, relative to Dync2h1, the BG01771 insertion site is within an intron near the middle of the coding region of the gene. Introduction of a splice acceptor, stop codons and an internal ribosome entry site for the Gal4 sequences is expected to truncate the Dync2h1 protein and, if it encodes btv, should produce the btv phenotype. However, despite the fact that, as we show in this paper, Dync2h1 does indeed encode the btv gene, the BG01771 insertion produces no detectable btv phenotype, as assayed by auditory electrophysiology (Table 1), and by the Drop Zone Assay (DZA) (Table 1; Fig. S2). Furthermore, BG01771 complements btv^1 and btv^2 in both of these assays. Finally, Gal4 expression, which should be under the control of Dvnc2h1, fails to drive any significant expression of UAS-lacZ or UAS-GFP (not shown).

To determine whether the *btv¹* lesion maps left or right of the *BG01771* insertion, we again conducted PIMR. Of nine recombinants recovered (Table S1), seven are consistent with *btv* mapping to the right of *BG01771*. However, two exceptional recombinants, one *Sp⁻ btv⁻ pr⁺* and one *Sp⁺ btv⁺ pr*, were recovered (Table S1). A lesion that inactivates the *btv* gene may explain the former, but the latter is more difficult to explain this way. More likely, these two recombinants represent gene conversions, which could only occur if the *btv¹* mutation is within a gene-conversion-tract distance from the *P*-element. PIMR initiates by a double-strand break at the *P*-element end, and is resolved by strand-recision, strand-invasion and repair. During this process, sequence differences, including substitutions, insertions and deletions, are efficiently converted if within the gene conversion tract length of less than 2 kb (Gloor et al., 1991, Preston and Engel, 1996). Therefore the *btv¹* mutation may be very close to the *BG01771* insertion site, likely to the right (based on the majority, 7 of 9, PIMR recombinants).

In the piggyBac insertional screen (Thibault et al., 2004), f06878 and f06884, two insertions of the WH element in the Dync2h1 and CG5674 region were recovered. One, f06878, is inserted just 6 bp left of the BG01771 insertion site (Fig. 5C, Table 1). Like BG01771, f06878 is within the Dync2h1 intron between exons 13 and 14, and in the 3' UTR of CG5674. Also like BG01771, f06878 has no detectable btv phenotype. In contrast, the f06884 insertion fails to complement btv¹ and btv⁰7109b. It is inserted in exon 23 of Dync2h1, which is also in the first intron of CG5674 (Fig. 5C; Table 1). That this insertion is responsible for the btv mutant phenotype was tested by making piggyBac transposase-mediated excisions. Three such excisions all reverted the btv mutant phenotype to the wild type (data not shown).

Together, these insertion alleles point to either Dync2h1 or CG5674 as the gene responsible for btv, and provide evidence against the four small genes to the right. However, because Dync2h1 and CG5674 are strongly mutually nested (Fig. 5C), it is imperative to distinguish them. Therefore, we took three approaches to distinguish these genes: generating imprecise excisions of transposon inserts, generating precise FLP-FRT mediated deletions, and sequencing the btv^{I} allele.

3. Imprecise excision: btv^{Lf234} derivative of BG01771

Screening for *P*-transposase-mediated excisions of the *BG01771* insertion resulted in many w⁻ derivatives. Unfortunately, none of these deleted any *Dync2h1* coding sequence; the majority of recovered events were partial excisions of the P-element, while the others appeared to be precise excisions. Because of the propensity for chromosomal rearrangements to occur by recombination between *P*-elements during hybrid dysgenesis, we generated heterozygotes between *BG01771* and the nearby *KG02815* insertion, in the presence of *P*-transposase. This approach, intended to generate a precise deletion between the insertion sites of *BG01771* and *KG02815* (Fig. 5B,C), instead yielded a cluster of three (later found to be identical) deletions. No flanking markers were used, so we cannot verify the mechanism of deletion generation, but the most likely event is a simple imprecise excision of the

BG01771 element without flanking exchange. The deletions, represented by btv^{Lf234} , (which we here rename btv^4) remove 3196 bp and insert a G nucleotide; they extend from 1377 bp left of the BG01771 insertion site rightward into the intron between exons 11-12 of Dync2h1 (Fig. 5C, Fig. S3). Thus btv^4 deletes two exons from Dync2h1 and introduces a frameshift. The btv^4 lesion is predicted to remove 60 C-terminal amino acids from the CG5674 gene product, replacing them through frame-shifting with 24 unrelated amino acids before termination. The three lines represented by btv^4 exhibited sedentary locomotor behavior, elevated DZA scores and electrophysiological deafness similar to the other btv alleles (Table 1). This further supports Dync2h1 or CG5674 as btv, but does not distinguish between them.

4. FLP-FRT-mediated deletions

With the availability of FRT-containing piggyBac insertions in the region, we used FLP-mediated recombination between nearby piggyBac insertions to generate precise deletions (Parks et al., 2004). Deletion #1 (del#1; Fig. 5C) was generated between the f06884 insertion near the 3' end of Dync2h1 and the f06319 insertion to the left of it. This removes about 104 kb including the first predicted exon of CG5674 and much of the last three predicted coding exons of Dync2h1. Deletion #2 (del#2; Fig. 1) removed about 19 kb, the region between f06878 rightward to f06603, which includes the first 13 exons of Dync2h1, as well as part of the 3' UTR of CG5674. Both del#1 and del#2 result in deafness and fail to complement other btv alleles. These results eliminate the four small genes to the right as candidates, leaving only CG5674 and, more likely, Dync2h1.

5. *btv*¹ deletes part of *Dync2h1* exon 13

Because btv^I was induced with EMS (EberlDuyk and Perrimon, 1997), we expected to find a single nucleotide mutation. Thus we tried to PCR-amplify DNA around the BG01771 insertion site from btv^I homozygotes for sequencing. However, several primer pairs which amplified products from the 40AG13 background strain failed to produce amplicons from btv^I DNA, suggesting a possible deletion around exon 13. Southern blot analysis using 3 different restriction enzymes (data not shown) was consistent with a ~400bp deletion. PCR using primers Se13F (in exon 13) and Dhc9R (in exon 9) produced a PCR product ~400bp smaller in btv^I than in 40AG13 DNA (Fig. 6A,B). Sequencing this product revealed a 401bp deletion along with a 6bp insertion (Fig. 6C). The deletion removes 125bp of Dync2h1 exon 13 and part of the intron between exons 12 and 13. Because this deleted region excludes any CG5674 sequences, the btv^I lesion firmly establishes Dync2h1 as btv.

Supplementary Figures

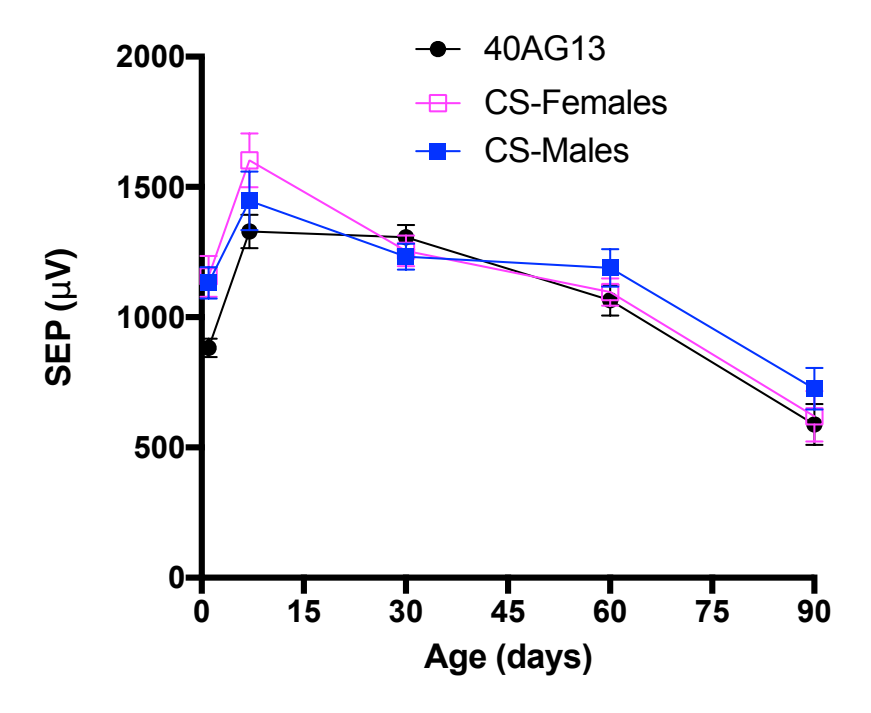


Figure S1. Age-dependent hearing loss in *Drosophila.* SEP recordings from the antennal nerve of Canton-S wild-type flies and the 40AG13 control strain. Depicted are the means \pm SD. For days 0 to 60, each data point represents 24-45 antennae, while at 90 days, each point represents 14-20 antennae.



Drop Zone Assay

Figure S2. Drop Zone Assay. The Drop Zone Assay (DZA) is a behavioral assay to quantitatively assess motor coordination that includes flying and walking behavior. Flies are introduced individually or 5 or 10 at a time into a 4-liter beaker, through a 1 inch hole in a plexiglass cover. After observing for 1 minute, flies are given a score between 1 and 6 as follows: 1 = fly flies and lands on the plexiglass cover, 2 = fly flies, lands on the side of the beaker and walks up to the cover, 3 = fly walks more than halfway up the wall of the beaker, 4 = fly walks less than halfway up the wall of the beaker, 5 = fly lands on bottom, walks around but does not walk up the wall of the beaker, 6 = fly lands on bottom and stays in position. Scores are averaged, and typical scores for wild-type flies are between 1 and 2, *btv* mutants typically score around 4, while *atonal* mutants score close to 6.

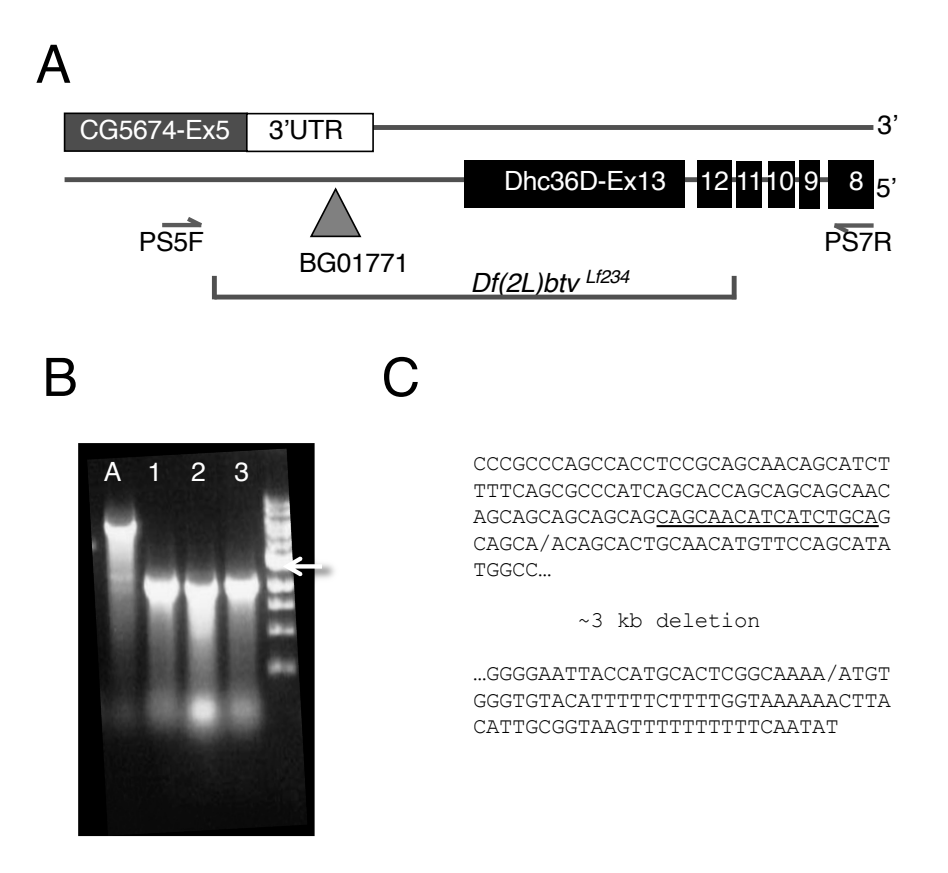


Figure S3. The *btv*^{*Lf234*} **deletion removes 3 kb affecting both** *Dync2h1* **and** *CG5674*. A) Map of central exons of *CG15148* (*Dync2h1*), with symbols as in Fig. 6. Positions of primers PS5F and PS7R used to confirm the deletion are indicated. The approximate position of the *btv*^{*Lf234*} deletion is shown by the bracketed region. B) Three deletion lines that arose as a cluster from a single dysgenic fly show the same deletion of about 3 kb. Panel shows PCR amplicons using primers shown in A to generate about a 5 kb band in the 40AG13 control (lane A), but only about 2 kb in the *Lf234*, *Lf245* and *Lf249* lines (Lanes 2, 3 and 4). C) Sequence analysis of the Lf234, Lf245 and Lf249 lines revealed identical deletions with 3196 nucleotides deleted and replaced with a single G nucleotide. Only the sequences of the ends of the deleted segment are shown, and the deletion breakpoints are indicated by forward slashes. The sequence corresponding to the PS5F primer is underlined.

MTQRTKFIINTSVEYFSARLPGSELDEQTAMILEFLEQEELTVISAVHSRSDGRIRFHHRIPNEELCLLFYKVPQVGHHR KEDGSEPLLGILTLEGGMVKSIYNSVSRVFSPSANSARRSEYGPELSGILENLHQNLGSSLGLPQSGITSLRNEIKYWQQ KLGOKSSSRLDREAAOVFIGVLENMEKOISTIDGANPSGTIEEFLDHAHTNLDELWRLPYNYPOORMADLLDIIGKRLLE VCLTQLLAEDVWSLNSSHVNNLMSQSIDTVDAWIQLCDSLTRLFWPNYVKHPWLGDSHVPKRGQQFKERLSEIRSIKQLY KQIATLLEDTELQEMFQEQAPFTEFNIFDTSSLGQNKWHKALQHFEQVLQPIDERIAAALKRQLHNHLSNPRQVIFIFSK YETLIQRPAVLELLTIEREQFLQSLHILLQDLRKAMVDSNMEPDTGHLSVICNECRWLKVVQHQIQEIEKVSHLISGREG FDKINKAVQEIKEETESLLRTNFEIWSGQCSTAVKSGELRLRDDQAVVKFEKEGRQLMRVTFNPKLVTFCQDVREFENLG YNVPLELRAAATHAAKYMCYARRLQQIATFHNTIGDRMIPCQRPIMLKNALELQRLVQSETVAWQDESSVQRYVDILQAA VSKLSSDNTLLVGYHEQAKRSVLKLMSTDLFTQNQIWKDELRHLRELVATLERQGYTHLDAFKLHWDHQLYKVLEYQYIL ${\tt GLLDMNNKLPDIHVKLVLRQRELVFSPPEEEIRELYFSQLRRFIERPCNFHGLSEHSQELFKSMVTVNRHHFGPLYQRAA}$ ELFDKLODFKTIWLPWIALGCVDVDOLCGIHLNEAGDWDRNFRSCKHFSOOLAKLOOAEESIDCIVINVLPLRSDIEYIS RRYWESLANSLRTAILTDVSLIQEFLQSALQFLQNVPMDEGSISQSGMKYEKIMSKLPQIEKTLEAVRAKDSCLGGWCKE RVTALSGILLQWEQLQPLLENHAVILQRQVDMIKNQAETQLQNLKNEAEKFLLRWESTISELEANEHSTLDVFKERRLHW QQLQEKKTQLLEECSKFNMEFPAEMLTPFTEIEEQMEKQSKQWQVYDSFLTELQPVLHEEWAIYRRRPYVLNEFIGKWEG SVHASIDLPSKRIROOVEOLOSALPILOOLOSESLSERHWARIFOLLNHKETKPLHSILLODILODFDVLOSAAOEISSI VRQASSEQIVRQALIELDQWSVTAQLKLITRTDASGQSVSLIKDYQEVLNKIGDNQSLLQSANNSAAFESFSDQAELWES RLNTLDALLSSLNHSQRRWVYLEPVFGSGTLQHEQALFKRIDKDFRFVMREIEMDPRVTSLTKINNITTIVNALETQLAR $\verb|CQQNLMSYITDKRNSFPRFYFLGDDLLELLGQASKDAEVIQRHIRKLFPGCHSLSIRQVGPNPATSSDVNQYSITSVHS|\\$ $\tt AEGDELKLSQPVEMKGDIERWLNQLVTVVQDTLRDQIYECYTGTTGGSDNLDEKILKKYASQVLATARALHFTRQAEQAI$ GSMSLGKLKQQLKDEITHLAALKNKSENGTLISLKLRALLLDLVHYSGVTEQLQKHNVVHTSDWHWLCQLRYYLGKKGGT SGEVNANRQVCVRMVYAEFEYAYEFLGQASKLVHTRLTHRCYLILTQAMHMGLGGNPF**GPAGTGKT**ECVKALGAMLGRLV LVFNCDENVDTESMSLILTGLARCGAWGCFDEFNRLQEATLSSISMLIQPIQSALKERANSVQIGERQIQLNQHCGIFVT $\verb|Lnpagaeyggroklpgniqalfrpivmoqpepgeiarvmlfvegfteasaiasrivelfelsgkmlsaqrhydwglrelk|$ TVLMVCGEGLRDQLTSEDNNQSSANFEMSVVVRCLRSSTMSKLAPHDVNRFEMLLRNVFPEIGSSPAPETQLHQSLSAAF ${\tt AQLGLCRSERQIEKALQLHEQLQKRMGVVLV} \underline{{\tt GPPGCGKS}} {\tt TIISLLKQALCGTQLKVHTISPKSMSRIQLLGRLDADTRQW}$ QDGVLTHTAVAVNQESSQVHSWIVCDGSIDPEWIEALNSVLDDNKLLTLPSGWRIQFGSNVNFIFETDDVRHASPATISR MGIVNMSYDYYPADGILKHELSKEPYGDLLQSYVDGKFQYAVNWIESQFLLTNHLPGINRAHLLRSLLLQLHGTQSLEEY GAATLRALFGYMPNDRQREFAQLILKHANLYVANPNYAELTHYESSRNSLEQYAVDAIETPEKGSQLIITSYMKSYLDIL $\verb|ETLLKTQGTRLPPFMLI| $\underline{\textbf{GPSGSGKT}}$ LLLQRAVLENSGYQLATINCSTQLTPRYILHTLKTHCVTVSGIKGREYRPKQARL | $\mathbf{C}_{\mathbf{C}}^{\mathsf{T}}$ and $\mathbf{C}_{\mathbf{C}^{\mathsf{T}}$ and $\mathbf{C}_{\mathbf{C}}^{\mathsf{T}}$ and $\mathbf{C}_{\mathbf{C}^{\mathsf{T}}$ and $\mathbf{C}_{\mathbf{C}}^{\mathsf{T}}$ and $\mathbf{C}_{\mathbf{C}}^{\mathsf{T}}$ and $\mathbf{C}_{\mathbf{C}}^{\mathsf{T}}$ and $\mathbf{C}_{\mathbf{C}}^{\mathsf{T}}$ and $\mathbf{C}_{\mathbf{C}}^{\mathsf{T}}$ and $\mathbf{C}_{\mathbf{C}}^{\mathsf{T}}$ and $\mathbf{C}_{\mathbf{C}^{\mathsf{T}}$ and $\mathbf{C}_{\mathbf{C}^{\mathsf{T}}$ and $\mathbf{C}_{\mathbf{C}^{\mathsf{T}}$ and $\mathbf{C}_{\mathbf{C}^{\mathsf{T}}$ and $\mathbf{C}_{\mathbf{C}^{\mathsf{T}}$ and \mathbf{C} VLFMKNLDLCOODSWGACEVVELLFOLAORGGFYAENLEWIGVSGLOLCASIGGNTGKIAPRYFAINOFVRVSRPTSODM $\tt LEIVQRRLEPLLEEHFRGSENRGRSGVNLQHVSESLMDCFEKLQATFTNVGGRQAHYQFSPKCIMKLLDALVFYPASDFNLOFFMANN AND STREET FOR ST$ EALYCELLGMFRDRLISEEHVOOFEGILKOTMRKYYGKEKVFFVPKSPKSRGHLHCLTHDEWMEEVOROVTICNTENYSI ${\tt TAPITEELLSHVARITRVLSRTDAHMLIL} \underline{{\tt GOSGGRHL}} {\tt DAIFTAATFQEAKVVTLQGGPSYDLTDFYNDLKVAMQTAALEQ}$ QMSYLLIEQCWLSYVPDILKPIEALLEGSEILELFGDDLETVASTLKQAAQLEGYQESMGTYFLKRARDYLHIIIVLDPN ${\tt SAKVQDYFNNFPALHRQMDLLYVRGESRETIAILPKQFIELLNESIAGGGSGRGKVPTCSHFADISDELPSEETSQRYYQ}$ LIRTYFHMYNNAANEIDQRLGKLQMGVDKLASAHALVDTLKSNAAAQEQALGEKRQLANEALEMISFTMRNANEQKSSML ELKQQTQKSSEQLKIRQKEIQQELAEVEPILAEASNAVGQIKSEALSEIRSLRAPPEAVRDILEGVLRLMGIRDTSWNSM KTFLAKRGVKEDIRSLDPARISPENCEAVERLLLAKGDSYEAKNAKRASAAAPLAAWVQASVRYSRVIQSIKPLEREQN ELQKNLNAAEDEMQELASGLDDVDKRVKQLSAKLQTYTQEAAVLELKLQEASGTLQAAELLVEKLSAEYTTWSLQLTELK ${\tt KAHKTLDAKTLLIAIAINYCAGLGLEQRCSSLKRLAADFHLPSDFDLRGSLLTEQQQIIWESQGLARDAQIIESAALLRE}$ $\verb|MLSLPYGACPIPLLLDPTQTAAAWLMAHLKGSGRPCELTTHGNDRLPYQLELAVRFGKTLLVTDCEQLRPPVLQLLQGHV|$ FVRFNKRQLAIGSKLVDLHESFQLVLISKSHRLDLPEEQRSQLNVLKFTVTAAGLADQLMSKAIVLKNGELEQQRIELLQ KEGHLLKQRMEMQDKLLEQLSKSEGDILKNEQLLESLNEIKQGSTQIDEALKQSGQIRDTLLAQFGSLRELSSRAATFYA ${\tt GLIQGYELSPLVYIELFLGALSKSQRDESKVYDCLVRSVYMNLARATSRDSQLSLSLWVCHQAYPDRLNPKEWELFVNNF}$ ${\tt MGSSDGSMVLSQLGKLPDCMPKEAQLKLAMLLQLFPDLRSKLQLEKDYIWRGFIEAQADDVLPALGSSFQRVLIAQIFRP}$ $\verb|DLMLHQLRKVSSDLLGISPDASTQPSVEQLLQQSSCDRPILMVSHAENDPTTELRKWANQKYREMAIGKGVEKRVLSEMR|$ QAAIDGHWLCVKNVHLVPEFLTQMERELSEIQKSKDFRLWLLCESTEGFSEAAIYKCLKVRYEQPKGLKQIVMRLLQNFA AEQDQKLKNQPKSLKMRLVYFVLTAVLQQRRQFIPQGWSKYYEFGEADLKAALGILRMMDQQLNSGKCDWLLMQRLSEAL AYGGRVNNQRDLEILTTYLNQFCSADVLSNRWSPLGLSLSIPTSGQLQDYYAALEKLPDTDEPSMYGLANQAQQQREIEQ AKRVIKELRGLHYGRGLAKDSGGAGESKGNDQLTGRQKLEQQIKPLLNLWRKLAASCTIIQTMKEAKTDVGESPWALFVLUGGARFANDERFORAELKLGADLYGIVHOTLSOMHAWLKESOEVDGSTLRTLAEOOIPASWLKLWPGPGSNSAVDFLRALIVRAOAAELRFREO MHLDFVEDINFVQVFNCENLLSCLKLLQSRKLAVSTERLELQTCGSSNLESDSSDIILKLAPLK//

1. VSKN (if no exon 25)

2. IDGAQSGMGKSNPFYIKYKIKDEVQNVSHTTTSSSKYGKNSLYSTQNAESKPKLPLYSRSSRDKLICHLNVDIVTGT AEQILLAGTALIVEDY (with exon 25)

Figure S4. The amino acid sequence of Dync2h1 encoded by the *btv* **gene.** Two possible translation start sites (see Fig. 5) are indicated, with the first generating a longer amino terminal end (red typeface). The selection of start sites has not been confirmed experimentally. The four predicted P-loop motifs are in bold underlined letters. At the carboxyl terminal, two possible terminal peptides are shown, depending on whether predicted exon 25 (see Fig. 5) is actually used. For the predicted form including the longer N and C termini, the predicted size of the entire protein is 481.45 kDa, consisting of 4237 amino acid residues.

```
P-loop 1
Hsap DKCYLTLTQAMKMGLGGNPYGPAGTGKTESVKALGGLLGRQVLVFNCD 1716
Rnor DKCYLTLTQAMKMGLGGNPYGPAGTGKTESVKALGGLLGRQVLVFNCD 1716
Tgra DKCYLTLTQGMHMGMGGNPYGPAGTGKTESVKALGGLFGRQVLVFNCD 1724
Cele
     DKCYLTLTQAMYMGLGGNPYGPAGTGKTESVKALAALMGRQVLVFNCD 1664
Crei DKCYLTLTOGMALGYGGNPYGPAGTGKTESVKALGOALAROVLVFNCD 1770
Agam HNCYLILTQAMQLGLGGNPFGPAGTGKTECVKSLGAMLGRLVLVFNCD 1625
Dmel HRCYLILTOAMHMGLGGNPFGPAGTGKTECVKALGAMLGRLVLVFNCD 1686
      P-loop 2
Hsap
     IKKALELYEQLCQRMGVVIVGPSGAGKSTLWRMLRAALCKTGKVVKQY 2006
Rnor MKKALELYEQLRQRTGVVIVGPSGAGKSTLWRMLRAALCKIGKVVKQY 2006
Tgra VKKALELYEOLRORMGVVVVGPSGSGKSTTWOILRAALNNTGOVVKOY 2016
Cele
     MEKVFOLYEOMRORIGVVVVGAAGSGKSTIWKILORSLILTKKPLKVT 1948
Crei IDRMLQLHLACEQRIGVIIVGPSGSGKSTLWELLEKAYERLGRKPIVY 2061
Agam VEKCLELQAQLQKRMGVVVIGPPQSGKTTIIALLKEALIAQGQIIRIH 1914
Dmel IEKALQLHEQLQKRMGVVLVGPPGCGKSTIISLLKQALCGT--QLKVH 1977
                 :* **:::<u>*.. .**:</u>*
                         P-loop 3
Hsap GLDYFKPWLSSDTKQPFILVGPEGCGKGMLLRYAFSQLRSTQIATVHC 2318
Rnor GLDYFKPWLSSETKQPFILVGPEGCGKGMLLRYAFSQLRSTEIATIHC 2318
     CLDFFNPWLEADNRQPFILVGPDGCGKGMVLRHCFAQLRSTQIATIHC 2328
     YSDIIGSWLOSGNRESFLITGTTGCGKOOLLKHCFONDPESOLASLYC 2253
Cele
     NLLMMAPWFK--NRDPFLVVGPEGCGKGALLDYCFKRIMGVQVAVVNC 2361
Crei
Agam DLLKHIIASK-E-RYVALLVGPSGNGKSLLLQTIVSEFSGYQLVTINC 2139
Dmel
     DILETLLKTQGTRLPPFMLIGPSGSGKTLLLQRAVLENSGYQLATINC 2285
                      :: <u>*. * **</u> :*
                                              ::. : *
                         P-loop 4
     EYMSRIDRVLSFPGGSLLLAGRSGVGRRTITSLVSHMHGAVLFSPKIS 2682
Hsap
     EYMSRIDRVLSFPGGSLLLAGRSGVGRRTVTSLVSHMHGAVLFSPKIS 2682
Rnor
Tgra DHVARVDRVLTQPRGSLLLAGRSGVGRRTAASLVAHCHRTELFSPNLS 2688
Cele FFCACIDRVLTGPGGHLFLPGRPGFGRRDSVRLVAHMHNIQVFSPPVT 2592
     ERVSRFDRVLSQQGGSLLLCGNSGVGRRSLMLLLAYMHNMDFITPKMT 2706
Agam ETIASIARALSRPYANLVMIGRAGSGRLOALYTACTMLNVRVAFPOMS 2467
Dmel SHVARITRVLSRTDAHMLILGQSGGRHLDAIFTAATFQEAKVVTLQGG 2617
        : . *.*:   . :.: <u>*..* :</u>
```

Figure S5. Conservation of four P-loops in Dync2h1. ClustalW was used to compare several Dync2h1 isoforms. The P-loop motifs are underlined and their positions are shown within the amino acid sequence context. The numbers at the end of each line reflect the amino acid position of the last residue in the line relative to the full-length annotation. The gi (gene identifier) numbers for these sequences are mentioned in the text. Only the sequences for the highly conserved P-loops are shown. Hsap, *Homo sapiens* gi:311033479; Rnor, *Rattus norvegicus* gi:12711694; Tgra, *Tripneustes gratilla* gi:17019507; Crei, *Chlamydomonas reinhardtii* gi:75337416; Cele, *Caenorhabditis elegans* gi:74963878; Agam, *Anopheles gambiae* gi:158298344. Small and hydrophobic residues (AVFPMILW) are shown in red, acidic residues (DE) are shown in blue, basic residues (RK) are shown in magenta, and residues with hydroxyl, sulfhydryl or amine side chains (STYHCNO), as well as glycine (G) are shown in green.

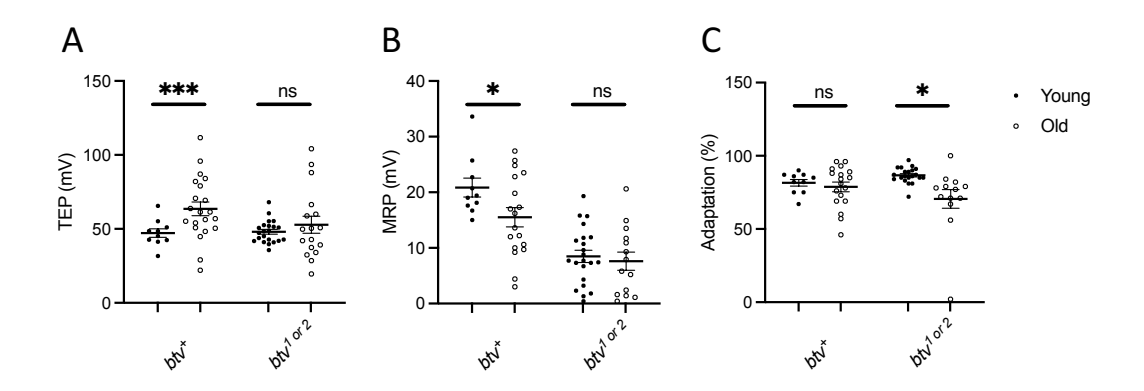


Figure S6. *btv* mutants do not undergo accelerated age-dependent degeneration in bristle organ function. A) TEPs in control flies are significantly enhanced in old flies (30 or more days old, open circles) compared to young flies (less than 5 days old, solid circles), but not in *btv* mutants. B) MRPs in control flies are significantly reduced with age, but age does not further reduce MRPs in *btv* mutants. C) Adaptation is not affected by age in control flies but shows a slight though significant decrease in *btv* mutants. For A-C, data from btv^{l} and btv^{l} are not significantly different and are thus pooled.

Supplementary Tables

Table S1. P-induced male recombination

Parental	Progeny	$Sp pr^+$	Sp^+pr	
genotype	screened	recombinants	recombinants	Interpretation
Sp btv ¹ pr rl cn/		8	4*	btv ¹ lesion is to the right of
$Sp^{+} KG08320 pr^{+}$	~2500	all btv ⁺	all btv⁻	KG08320.
Sp btv ¹ pr rl cn/		5	4	btv ¹ likely to the right of, but
$Sp^{+}BG01771 pr^{+}$	5966	4 btv ⁺ , 1 btv ⁻	1 btv ⁺ , 3 btv ⁻	very close to, BG01771.

^{*} One Sp^+pr recombinant is a large deletion from the KG08320 insertion site extending rightward to at least M(2)36F, including btv and rdo. We named this Df(2L)P2.

Table S2. Polymorphisms in the btv gene coding sequence

nnotated Feature	40AG13	w ¹¹¹⁸
R237		R237R
A409	A409T	A409T
F503	F503F	F503F
Q602		Q602R
Q614	Q614Q	Q614Q
S619	S619S	S619S
L636	L636L	L636L
L729	L729L	L729L
N769		N769N
Q807	Q807E	Q807E
D823	D823D	D823D
K936	K936E	
G955	G955A	G955A
Q1000	Q1000Q	Q1000Q
L1013	L1013L	L1013L
H1027	H1027H	H1027H
L1038	L1038F	L1038F
S1080	S1080S	S1080S
D1087		D1087G
V1096	V1096I	V1096I
E1153	E1153D	E1153D
S1154	S1154S	S1154S
E1196		E1196G
Q1208	Q1208H	Q1208H
T1232	-	T1232A
I1242	I1242I	I1242I
N1263	N1263K	N1263K
R1330	R1330R	R1330R
K1670	K1670K	K1670K
T1806	T1806T	T1806T
N2127	N2127K	N2127K
L2139	L2139F	L2139F
N2205	N2205N	N2205N
I2238	I2238L	
F2456	F2456S	
E2706	E2706E	
H2744	H2744H	
Q2805	Q2805Q	
F3564	F3564C	
R3568	R3568Q	
S3569	S3569I	
N3702	N3702N	

Note: Polymorphisms found in the two lab strains 40AG13 and w¹¹¹⁸ are listed according to their effect on the *Dync2h1* amino acid sequence, encoded by the *btv* gene, with respect to the annotated sequence generated in the fly genome project. Synonymous mutations are listed in black typeface, non-synonymous changes are shown in red.

References cited in Supplementary Material

- CALDWELL, J. C., FINEBERG, S. K. & EBERL, D. F. 2007. reduced ocelli encodes the leucine rich repeat protein *Pray For Elves* in *Drosophila melanogaster*. Fly, 1, 146-152.
- CALDWELL, J. C., MILLER, M. M., WING, S., SOLL, D. R. & EBERL, D. F. 2003. Dynamic analysis of larval locomotion in *Drosophila* chordotonal organ mutants. *Proceedings of the National Academy of Sciences (U.S.A.)*, 100, 16053-16058.
- CHEN, B., CHU, T., HARMS, E., GERGEN, J. P. & STRICKLAND, S. 1998. Mapping of Drosophila mutations using site-specific male recombination. *Genetics*, 149, 157-163.
- COMERON, J. M., REED, J., CHRISTIE, M., JACOBS, J. S., DIERDORFF, J., EBERL, D. F. & MANAK, J. R. 2016. A Mismatch EndoNuclease Array-based Methodology (MENA) for identifying known SNPs or novel point mutations. *Microarrays (Basel)*, 5, E7.
- EBERL, D. F., DUYK, G. M. & PERRIMON, N. 1997. A genetic screen for mutations that disrupt an auditory response in *Drosophila melanogaster*. *Proceedings of the National Academy of Sciences* (U.S.A.), 94, 14837-14842.
- EBERL, D. F., HARDY, R. W. & KERNAN, M. 2000. Genetically similar transduction mechanisms for touch and hearing in *Drosophila*. *Journal of Neuroscience*, 20, 5981-5988.
- GLOOR, G. B., NASSIF, N. A., JOHNSON-SCHLITZ, D. M., PRESTON, C. R. & ENGELS, W. R. 1991. Targeted gene replacement in *Drosophila* via P element-induced gap repair. *Science*, 253, 1110-1117.
- LUKACSOVICH, T., ASZTALOS, Z., AWANO, W., BABA, K., KONDO, S., NIWA, S. & YAMAMOTO, D. 2001. Dual-tagging gene trap of novel genes in *Drosophila melanogaster*. *Genetics*, 157, 727-742.
- MANCEBO, R., ZHOU, X., SHILLINGLAW, W., HENZEL, W. & MACDONALD, P. M. 2001. BSF binds specifically to the *bicoid* mRNA 3' untranslated region and contributes to stabilization of *bicoid* mRNA. *Molecular and Cellular Biology*, 21, 3462-3471.
- PARKS, A. L., COOK, K. R., BELVIN, M., DOMPE, N. A., FAWCETT, R., HUPPERT, K., TAN, L. R., WINTER, C. G., BOGART, K. P., DEAL, J. E., DEAL-HERR, M. E., GRANT, D., MARCINKO, M., MIYAZAKI, W. Y., ROBERTSON, S., SHAW, K. J., TABIOS, M., VYSOTSKAIA, V., ZHAO, L., ANDRADE, R. S., EDGAR, K. A., HOWIE, E., KILLPACK, K., MILASH, B., NORTON, A., THAO, D., WHITTAKER, K., WINNER, M. A., FRIEDMAN, L., MARGOLIS, J., SINGER, M. A., KOPCZYNSKI, C., CURTIS, D., KAUFMAN, T. C., PLOWMAN, G. D., DUYK, G. & FRANCIS-LANG, H. L. 2004. Systematic generation of high-resolution deletion coverage of the *Drosophila melanogaster* genome. *Nature Genetics*, 36, 288-292.
- PRESTON, C. R. & ENGEL, W. R. 1996. *P*-element-induced male recombination and gene conversion in Drosophila. *Genetics*, 144, 1611-1622.
- SPRADLING, A. C., STERN, D., BEATON, A., RHEM, E. J., LAVERTY, T., MOZDEN, N., MISRA, S. & RUBIN, G. M. 1999. The Berkeley Drosophila Genome Project gene disruption project: single *P*-element insertions mutating 25% of vital Drosophila genes. *Genetics*, 153, 135-177.
- THIBAULT, S. T., SINGER, M. A., MIYAZAKI, W. Y., MILASH, B., DOMPE, N. A., SINGH, C. M., BUCHHOLZ, R., DEMSKY, M., FAWCETT, R., FRANCIS-LANG, H. L., RYNER, L., CHEUNG, L. M., CHONG, A., ERICKSON, C., FISHER, W. W., GREER, K., HARTOUNI, S. R., HOWIE, E., JAKKULA, L., JOO, D., KILLPACK, K., LAUFER, A., MAZZOTTA, J., SMITH, R. D., STEVENS, L. M., STUBER, C., TAN, L. R., VENTURA, R., WOO, A., ZAKRAJSEK, I., ZHAO, L., CHEN, F., SWIMMER, C., KOPCZYNSKI, C., DUYK, G., WINBERG, M. L. & MARGOLIS, J. 2004. A complementary transposon tool kit for *Drosophila melanogaster* using *P* and *piggyBac*. *Nature Genetics*, 36, 283-287.
- TÖRÖK, T., TICK, G., ALVARADO, M. & KISS, I. 1993. *P-lacW* insertional mutagenesis on the second chromosome of *Drosophila melanogaster*: Isolation of lethals with different overgrowth phenotypes. *Genetics*, 135, 71-80.